

UNIVERSITY OF SOUTHAMPTON

**Disc Winds Matter: Modelling
Accretion and Outflow on All Scales**

by

James Matthews

A thesis submitted in partial fulfillment for the
degree of Doctor of Philosophy

in the
Faculty of Physical Sciences and Engineering
Department of Physics & Astronomy

March 2016

“Here, on the edge of what we know, in contact with the ocean of the unknown, shines the mystery and the beauty of the world.

And it’s breathtaking.”

Seven Brief Lessons on Physics, Carlo Rovelli

“Good enough for government work.”

Christian Knigge

UNIVERSITY OF SOUTHAMPTON

Abstract

Faculty of Physical Sciences and Engineering

Department of Physics & Astronomy

Doctor of Philosophy

by James Matthews

The Thesis Abstract is written here (and usually kept to just this page). The page is kept centered vertically so can expand into the blank space above the title too...

Acknowledgements

Contents

| | |
|--|------------|
| Abstract | ii |
| Acknowledgements | iii |
| 1 Introduction | 1 |
| 1.1 The Physics of Accretion | 3 |
| 1.1.1 Spherical Accretion and The Eddington Limit | 3 |
| 1.1.2 Accretion Discs | 5 |
| 1.1.2.1 Steady-state Accretion Discs: The α -prescription | 5 |
| 1.2 Accreting Compact Binaries | 7 |
| 1.2.1 Roche Lobe-Overflow | 8 |
| 1.2.2 Cataclysmic Variables | 9 |
| 1.2.2.1 Dwarf Novae and the Disc-instability Model | 9 |
| 1.2.2.2 Nova-like Variables | 10 |
| 1.2.3 Low Mass X-ray Binaries | 13 |
| 1.3 Quasars and Active Galactic Nuclei | 13 |
| 1.3.1 AGN Taxonomy | 14 |
| 1.3.1.1 Radio Galaxies | 14 |
| 1.3.1.2 BL Lacs and Blazars | 14 |
| 1.3.1.3 Obscured and Compton-thick AGN | 16 |
| 1.3.1.4 Low-luminosity AGN | 16 |
| 1.3.2 AGN Unification and the dusty Torus | 16 |
| 1.3.3 X-ray Properties of AGN | 18 |
| 1.3.4 The Broad Line Region and Connection to Outflows | 18 |
| 1.4 The Current Understanding of the Disc Continuum | 19 |
| 1.4.1 The Spectral shape of CV discs | 20 |
| 1.4.2 The Big Blue Bump in AGN | 20 |
| 1.4.2.1 Fitting AGN Spectra | 20 |
| 1.4.2.2 The 1000Å Break | 20 |
| 1.4.2.3 The Accretion Disc Size Problem | 20 |
| 1.4.2.4 The Soft-Xray Excess | 21 |
| 1.5 The Universality of Accretion | 21 |
| 1.5.1 The RMS-flux relation | 21 |
| 1.5.2 Accretion States | 21 |
| 1.5.3 Jets and Outflows | 21 |
| 1.5.4 A Global Picture | 21 |

| | |
|--|-----------|
| 2 Accretion Disc Winds | 23 |
| 2.1 Accretion Disc Winds: Observational Evidence | 23 |
| 2.1.1 Cataclysmic Variables | 23 |
| 2.1.2 X-ray Binaries | 23 |
| 2.1.3 AGN and Quasars | 23 |
| 2.1.3.1 Broad Absorption Line Quasars | 23 |
| 2.1.3.2 Warm Absorbers | 23 |
| 2.1.3.3 Ultra-fast Outflows | 23 |
| 2.1.4 Stellar Winds | 23 |
| 2.1.4.1 Clumping | 23 |
| 2.2 Accretion Disc Winds: Driving Mechanisms | 23 |
| 2.2.1 Thermal Winds | 24 |
| 2.2.2 Radiatively Driven Winds | 25 |
| 2.2.3 Line-driven Winds | 25 |
| 2.2.4 Magneto-centrifugal Winds | 25 |
| 2.3 Accretion Disc Wind Models | 25 |
| 2.4 A Kinematic Prescription | 25 |
| 2.5 The really, really big picture: AGN Feedback | 25 |
| 2.5.1 Observational evidence for feedback | 25 |
| 2.5.2 Radiative or quasar mode feedback | 27 |
| 2.5.3 Kinetic or radio mode feedback | 27 |
| 2.5.4 In-situ Explanations | 27 |
| 3 Radiative Transfer and Ionization | 28 |
| 3.1 Fundamentals of Radiative Transfer | 28 |
| 3.1.1 Spectral Line Formation | 30 |
| 3.1.2 The Two Level Atom | 30 |
| 3.1.2.1 Einstein Coefficients | 30 |
| 3.1.2.2 Collision Strengths | 31 |
| 3.1.3 The Sobolev Approximation | 31 |
| 3.1.3.1 Escape Probabilities | 32 |
| 3.1.4 Monte Carlo approaches | 32 |
| 3.2 PYTHON: A Monte Carlo Ionization and Radiative Transfer Code | 32 |
| 3.2.1 Basics | 32 |
| 3.3 Macro-atoms | 34 |
| 3.3.1 Macro-Atom Estimators | 36 |
| 3.3.1.1 Radiation Field Estimators | 36 |
| 3.3.1.2 Heating And Cooling Estimators | 36 |
| 3.3.2 Ionization Fractions and Level Populations | 36 |
| 3.4 Simple-atoms | 36 |
| 3.5 Heating And Cooling | 36 |
| 3.5.1 Heating And Cooling Balance | 36 |
| 3.5.2 Heating And Cooling Estimators | 36 |
| 3.5.2.1 Macro-atoms | 36 |
| 3.5.2.2 Simple-atoms | 37 |
| 3.6 Spectral Synthesis | 38 |
| 3.7 Atomic Data | 38 |

| | | |
|-------------------------|--|---------------|
| 3.8 | Clumping | 39 |
| 3.8.1 | Motivation | 39 |
| 3.8.2 | Microclumping | 40 |
| 3.9 | Code Validation | 41 |
| 3.9.1 | Testing against Cloudy | 41 |
| 3.9.2 | Testing against Tardis | 41 |
| 3.10 | Code Maintenance and Version Control | 41 |
| 3.10.1 | Parallelisation | 41 |
| Bibliography | | 42 |

Chapter 1

Introduction

“And now you’re asking, I don’t know where to begin”

Mike Vennart, Silent/Transparent

The release of gravitational potential energy as mass falls towards a compact object is the most efficient energetic process in the universe, capable of liberating more rest mass energy than nuclear fusion. This *accretion* process is thought to power the huge radiative engines at the centres of every galaxy – accreting supermassive black holes known as active galactic nuclei (AGN). As the matter falls into the potential well of the black hole it often forms an accretion disc, which, in many cases, is an efficient radiator of the gravitational energy released. In some cases, the accretion disc can outshine the entire stellar population of the galaxy, appearing as a quasi-stellar object (QSOS) or *quasar*. In addition to AGN, accretion discs are present in X-ray binaries (XRBs), young-stellar objects (YSOs) and cataclysmic variables (CVs). Accretion is a universal process; broadly speaking, the physics is similar of whether matter is falling on to a $\sim 1 M_\odot$ Neutron Star or White Dwarf system, or a $\sim 10^{10} M_\odot$ black hole.

Outflows are ubiquitous in accreting systems. We see collimated radio jets in AGN (Hazard et al. 1963; Potash and Wardle 1980; Perley et al. 1984; Marscher 2006) and XRBs (Belloni 2010), and there is even evidence of extended radio emission in CVs (Benz et al. 1983; Coppejans et al. 2015). These radio jets tend to appear in specific accretion states (Fender 2001; Körding et al. 2008), implying an intrinsic connection to the accretion process. Even more intriguing, in XRBs less collimated, mass-loaded outflows or *winds* are observed in the opposite accretion state, possibly emanating from the accretion disc. Evidence for disc winds is widespread across the mass range, but perhaps the most spectacular indication is the blue-shifted, broad absorption lines (BALs) in the rest-frame ultraviolet (UV) seen in high-state CVs (Heap et al. 1978; Greenstein and Oke 1982;

Cordova and Mason 1982) and the so-called broad absorption line quasars (BALQSOs) that make up 20 – 40% of quasars (Weymann et al. 1991; Knigge et al. 2008; Allen et al. 2011). BALs and ‘P-Cygni’ profiles (Struve 1935; Rottenberg 1952) are also seen in stellar winds (e.g. Cassinelli 1979) and sometimes even in the optical spectra of CVs (Patterson et al. 1996; Ringwald and Naylor 1998; Kafka and Honeycutt 2004). Broad, blue-shifted absorption is even observed in the Fe K α line in AGN (Reeves et al. 2003; Pounds and Reeves 2009; Tombesi et al. 2010) – these are known as ultra-fast outflows or UFOs¹.

The astrophysical significance of disc winds extends, quite literally, far beyond the accretion environment. They offer a potential mechanism by which the central accretion engine can interact with the host galaxy and interstellar medium via a ‘feedback’ mechanism (King 2003; Fabian 2012). Feedback is required in models of galaxy evolution (Springel et al. 2005) and may explain the famous ‘ $M - \sigma$ ’ relation (Silk and Rees 1998; Häring and Rix 2004). Winds also offer a natural way to *unify* much of the diverse phenomenology of AGN, CVs and XRBs. The principle of unification can be applied along more than one ‘axis’ of parameter space. For example, there exist elegant models that attempt to explain *all* of the behaviour of quasars with only a central black hole, a jet, an accretion disc, and an associated outflow, by varying the viewing angle (Elvis 2000). Similarly elegantly, it has been shown that much of the behaviour of XRBs is directly applicable to AGN (McHardy et al. 2006), and models of outflows in CVs have been successfully ‘scaled-up’ and applied to quasars and AGN (e.g. Higginbottom et al. 2013).

Despite their clear importance and ubiquity, there are still many unanswered questions relating to the true impact of winds and their underlying physical origins. Here, I aim to address some of these questions, and take steps towards building a more holistic picture of the impact of winds on the spectral appearance and accretion physics of disc systems. This thesis is structured as follows. In the remainder of this chapter, I will give the background accretion theory and detail the successes and failures of accretion disc models when compared to observations, as well as describing the different classes of accreting objects in more detail. In chapter 2, I dedicate some time to specifically discussing the theory of, and observational evidence for, accretion disc winds. In chapter 3, I outline the Monte Carlo radiative transfer (MCRT) and photoionization methods I have used in order to investigate the impact of disc winds on the spectra of accreting systems. The science chapters contain three separate submitted papers, in which we investigated the impact of disc winds on the spectra of CVs (Chapter 5), and tested disc wind quasar unification models (Chapters 6 and 7). In chapter 8, I summarise my

¹It should be noted that, while X-ray spectral fitting can be somewhat of a dark art, the explanations for these UFOs are somewhat more believable than their sci-fi namesakes.

findings and their astrophysical significance, and discuss potential avenues for future work.

1.1 The Physics of Accretion

The basic phenomenon of accretion- matter falling into a gravitational potential well- is a ubiquitous one in astrophysics. The energy, ΔE , released by a parcel of mass Δm falling from infinity onto an object of mass M and radius R_* is given by

$$\Delta E = \frac{GM\Delta m}{R_*}, \quad (1.1)$$

meaning that the accretion power can then be given by

$$L_{acc} = \frac{G M \dot{M}}{R}. \quad (1.2)$$

We can also parameterise any energetic process with the form

$$\Delta E = \eta \dot{M} c^2, \quad (1.3)$$

where η is some efficiency. Nuclear fusion is one of the more efficient energetic processes in the universe, with an efficient of $\eta = 0.007$. If we rearrange the above equations in terms of η we find

$$\eta = \frac{G}{c^2} \frac{M}{R}. \quad (1.4)$$

In other words, the efficiency of accretion is directly related to the *compactness* of the central object. Values of compactness for four different compact objects are shown in table ??.

1.1.1 Spherical Accretion and The Eddington Limit

The simplest geometry one might propose for accretion would be one in which a central mass accretes matter from an all-encompassing cloud or the inter-stellar medium. The process of spherical accretion has come to be known as Bondi-Hoyle-Lyttleton accretion ([Hoyle and Lyttleton 1939](#); [Bondi and Hoyle 1944](#)). In particular, [Bondi \(1952\)](#) studied spherically symmetric accretion onto a point mass and derived the Bondi radius,

$$r_B = \frac{GM}{c_S^2}, \quad (1.5)$$

where $c_S = c_S(r_B)$ is the sound speed as a function of radius. The Bondi radius represents a critical point inside which the material is supersonic and will accrete on the free-fall timescale.

If this timescale is long enough, then the accreting matter can radiate its potential energy with luminosity L . This radiation can induce a force on free electrons, given by

$$F_{rad} = \frac{L\sigma_T}{4\pi r^2 c}, \quad (1.6)$$

where $\sigma_T = 6.65 \times 10^{-25} \text{ cm}^2$ is the Thomson cross-section. If this radiation force term dominates over the gravitational force then the material will no longer fall inwards. Consider radiation pressure acting on electron-proton pairs, for which the gravitational force is approximately given by GMm_p/r^2 . Combining this expression with equation 1.6 gives a natural maximum accretion luminosity, known as the *Eddington limit*, of

$$L_{Edd} = \frac{4\pi GMm_p c}{\sigma_T}, \quad (1.7)$$

with an associated Eddington accretion rate of

$$\dot{M}_{Edd} = \frac{L_{Edd}}{\eta c^2}. \quad (1.8)$$

The Eddington limit makes a number of assumptions, namely that the accretion flow is steady, spherically symmetric, ionized, and has its opacities dominated by electron scattering. Clearly, there are many astrophysical situations where this does not hold. For example, the recent outburst of V404 Cyg showed wildly variable luminosities on short timescales (see, e.g., [Kuulkers et al. 2015](#); [Motta et al. 2015](#), among many, many ATels), and in any binary system or disc dominated system then the assumption of spherical symmetry will break down. Nevertheless, the Eddington limit gives a good order of magnitude estimate of the maximum luminosity of an accreting object, and also provides a useful way of parameterising accretion rate, as it scales linearly with mass. It can also be used to characterise the *state* of an accretion disc. In general, sources around 0.1 L_{Edd} find themselves in a soft or thin-disc state (REFs), whereas for much lower Eddington fractions sources will be dominated by advection and form radiatively-inefficient accretion flows (RIAFs; REFs). It is also clear that around the Eddington limit radiation pressure must play a major role in determining the disc morphology (see section 2.2.2).

1.1.2 Accretion Discs

In many astrophysical situations – for example, binary orbits and gas clouds orbiting gas clouds – any accreting matter will possess some net angular momentum. If the medium is dense enough, then collisions between particles will be frequent, and the total angular momentum vector of two colliding particles will always be conserved. This allows a mechanism for a gas cloud to relax to its minimum energy state – an accretion disc.

As well as losing gravitational potential energy as it falls towards the central mass, a parcel of matter must always lose this angular momentum. Crucially, accretion discs provide a way for a given parcel of mass to lose angular momentum. If the disc itself maintains the same total angular momentum, then it follows that angular momentum must therefore be transported outwards.

1.1.2.1 Steady-state Accretion Discs: The α -prescription

The so-called α -disc model developed by ([Shakura and Sunyaev 1973](#), hereafter SS73) and [Lynden-Bell \(1969\)](#) is currently the leading candidate for explaining how energy and angular momentum is transported an accretion disc. The starting point for this model is the parameterisation of viscosity using a simple form of

$$\nu = \alpha c_s H. \quad (1.9)$$

Viscous torques then allow the conversion of orbital kinetic energy into heat, which can be radiated away. If we then make one further assumption, that the accretion rate is constant throughout the disc, then we can write down a mass continuity equation valid at all radii, given by

$$\dot{M} \equiv 2\pi R V_R \Sigma = 0 \quad (1.10)$$

where Σ is the surface density at that point. The angular momentum equation becomes, in this case

$$\nu' \Sigma = \frac{\dot{M}}{3\pi} \left[1 - \left(\frac{R}{R_*} \right)^{1/2} \right] \quad (1.11)$$

The viscous torques throughout the disc cause a local loss of mechanical energy, allowing one to derive (see, e.g. [Frank et al. 1992](#)) a rate of viscous dissipation, per unit area, given by

$$D(R) = \frac{1}{2} \nu' \Sigma (R \Omega')^2. \quad (1.12)$$

Here, $D(R)$ is proportional to the derivative of the angular velocity, $\Omega' = d\Omega/dR$. By combining equations 1.12 and 1.11 we can show that the viscous dissipation rate is

$$D(R) = \frac{GMM}{8\pi R^3} \left[1 - \left(\frac{R}{R_*} \right)^{1/2} \right] \quad (1.13)$$

where we have also set the angular velocity to the Keplerian velocity. This expression is, importantly, independent of viscosity – which is fortunate, because we do not know what value of α to use in equation 1.9. This result comes about because of the implicit assumption that the viscosity regulates the mass accretion rate so as to achieve a steady state.

We can now integrate across the whole disc to obtain the disc luminosity,

$$L_{disc} = 2 \int_{R_*}^{\infty} D(R) 2\pi R dR = \frac{GMM}{2R_*} = \frac{1}{2} L_{acc}. \quad (1.14)$$

This result can also be shown by considering the binding energy of gas at R_* and infinity. From equation 1.13 one can also derive an effective temperature distribution, by setting

$$\sigma T_{eff}^4(R) = D(R), \quad (1.15)$$

which then gives

$$T_{eff}(R) = T_* \left[1 - \left(\frac{R}{R_*} \right)^{1/2} \right]^{1/4}, \quad (1.16)$$

where

$$T_* = \left(\frac{3GMM}{8\pi R_*^3 \sigma} \right)^{1/4}. \quad (1.17)$$

When $R \gg R_*$ then we can simplify this to

$$T_{eff}(R) = T_* (R/R_*)^{-3/4}. \quad (1.18)$$

Now we have not only derived the total luminosity of an accretion disc, but also the effective temperature profile which will govern the shape of the emergent SED. This temperature profile is shown in figure 1.1 for the same four objects shown in table ??, assuming an Eddington fraction of 0.2.

It is important to recognise that the steady-state disc treatment *does not specify the nature of the disc SED*. What it does do is say where energy is originally released. Typically, accretion discs are modelled as a series of annuli each emitting as blackbodies, but a disc atmosphere with frequency-dependent opacity would create a somewhat different spectrum. Figure ? shows the blackbody SEDs expected for the same objects as

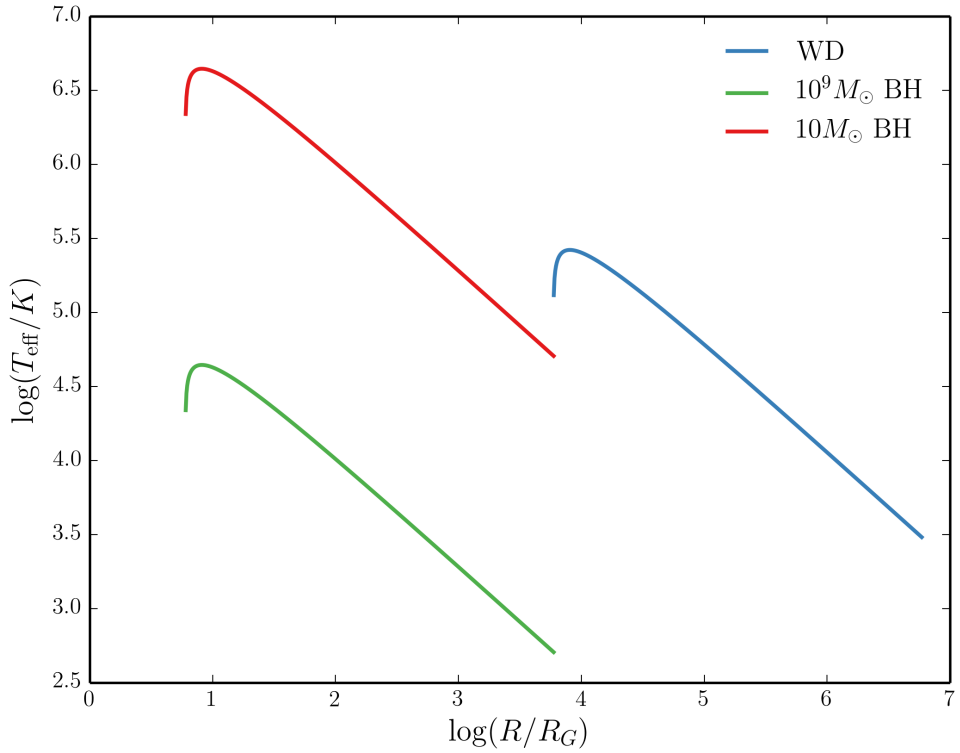


FIGURE 1.1: The temperature profile of an accretion disc for three different classes of compact object.

figure 1.1. Figure ? shows a comparison between a disc atmosphere model and black-body model for a cataclysmic variable accretion disc, showing the differences in spectral shape caused by frequency-dependent opacities in the disc. It is of course possible that *neither* blackbody or disc atmosphere treatments are realistic. I shall therefore devote a little time to discussing the observational arguments for accretion discs and the different classes of accreting objects.

1.2 Accreting Compact Binaries

Accreting compact binaries form many different classes, but are all characterised by matter streaming from a donor star or secondary onto a compact object or primary. There are only two ways by which matter can transfer from the secondary to the compact object. One is by Roche Lobe-overflow (RLOF), whereby stellar evolution causes the donor star to fill its Roche Lobe, the surface of equipotential around the star. The alternative is that the donor may expel material via a disc around the secondary or radiatively driven stellar wind, allowing some of it to flow onto the compact object. Although accretion from a wind or circumstellar disc is common in such as high-mass

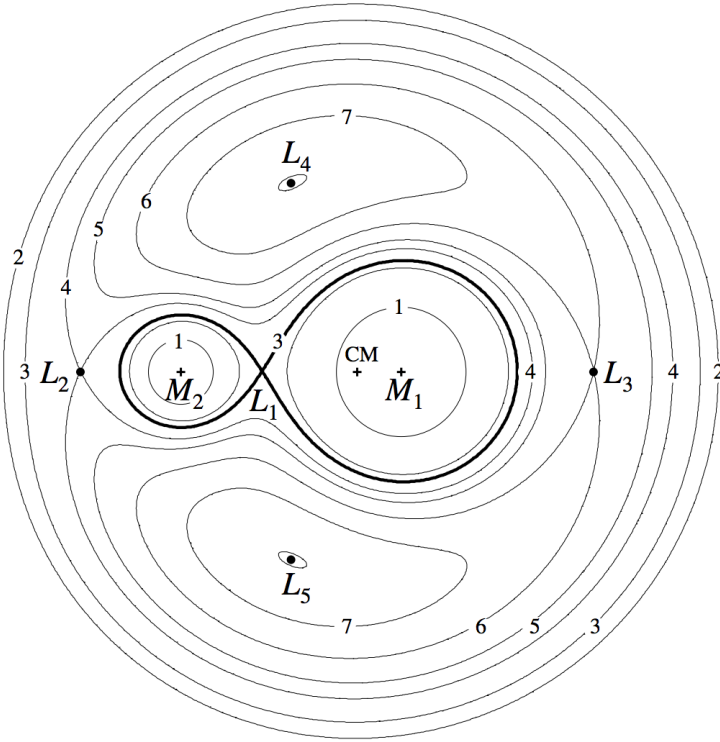


FIGURE 1.2: Credit: Frank et al. 2002. The Roche potential in a binary system for $q = M_2/M_1$ of 0.25. The Lagrangian points are marked, as are the locations of the individual and system centres of mass.

X-ray binaries (HMXBs; e.g. [Bartlett 2013](#)), here I will focus on RLOF as it is more common in the systems that commonly exhibit high-state accretion discs and associated outflows.

1.2.1 Roche Lobe-Overflow

Let us consider a binary system, with masses M_1 and M_2 , at positions \vec{r}_1 and \vec{r}_2 . The Roche potential, Φ_R , in this system is then

$$\Phi_R = -\frac{GM_1}{|\vec{r} - \vec{r}_1|} - \frac{GM_2}{|\vec{r} - \vec{r}_2|} - 1/2(\vec{\omega} \times \vec{r})^2, \quad (1.19)$$

where $\vec{\omega}$ is the angular velocity of the binary and is a vector normal to the orbital plane. This potential is plotted in figure 1.2 for a mass ratio, $q = M_2/M_1$ of 0.25.

In the context of semi-detached binary systems, the most important region of the potential is the dumbbell shaped region enclosing the masses. Each of these enclosed regions is known as the ‘Roche lobe’ of the object and can be expressed approximately in terms of the mass ratio and separation of the system. An approximation for the size of the

Roche lobe takes the form ([Eggleton 1983](#))

$$\frac{R_2}{a} = \frac{0.49q^{2/3}}{0.6q^{2/3} + \ln(1 + q^{1/3})}. \quad (1.20)$$

Here R_2 is the radius of a sphere with the same volume as the Roche lobe for the secondary star, which we can see depends only on q and the orbital separation, a . If this secondary expands enough to fill its Roche lobe, then matter will fall onto the other object. This process is known as Roche Lobe overflow (RLOF), and is vitally important in astrophysics. Although caused by stellar evolution, it affects the mass ratio of the binary system and thus itself affects the evolution of binary systems. This has serious ramifications for the orbital period distribution of binaries (REFs) as well as affecting the delay time distribution of Type Ia Supernovae, for which CVs are one of the progenitor candidates. It is also worth noting that the existence of gravitational waves has been required in models for CV evolution since

1.2.2 Cataclysmic Variables

Cataclysmic variables (CVs) are systems in which a WD accretes matter from a donor star via Roche-lobe overflow (see the ‘CV bible’, [Warner 2003](#)). CVs are not always dominated by their accretion luminosity; classical novae and super soft sources (SSS) emit mostly due to nuclear burning on the WD surface. *Accreting* CVs – the focus here – can be classified according to the magnetic field strength (B) and photometric activity. Magnetic systems are classified as either ‘Polars’ ($B \gtrsim 10^7$ G) or ‘Intermediate Polars’ ($10^6 \lesssim B \lesssim 10^7$ G); in these systems the accretion flow inside the some critical radius (related to the Alfvén radius) is dominated by the WDs magnetic field (e.g. [Patterson 1994](#)). In polars this radius is large enough, due to the strong magnetic field, that no disc forms at all ([Liebert and Stockman 1985](#)). When $B \lesssim 10^6$ G then the accreting material can fall onto the WD via a disc, and the CV is classified as non-magnetic. There are a two main types of non-magnetic CVs; Dwarf Novae and Nova-like variables.

1.2.2.1 Dwarf Novae and the Disc-instability Model

Dwarf novae (DNe) are CVs that are characterised by repeated periods of quiescence and dramatic outburst. One of the most famous DNe is SS Cyg, whose light curve is shown in figure 1.3. The repeated outbursts can be clearly seen, and SS Cyg itself has been undergoing this behaviour for the full century for which it has been observed. A spectrum over the course of a typical outburst is shown in figure 1.4, and is characterised by the appearance of an optically thick accretion disc continuum – note the similarity to

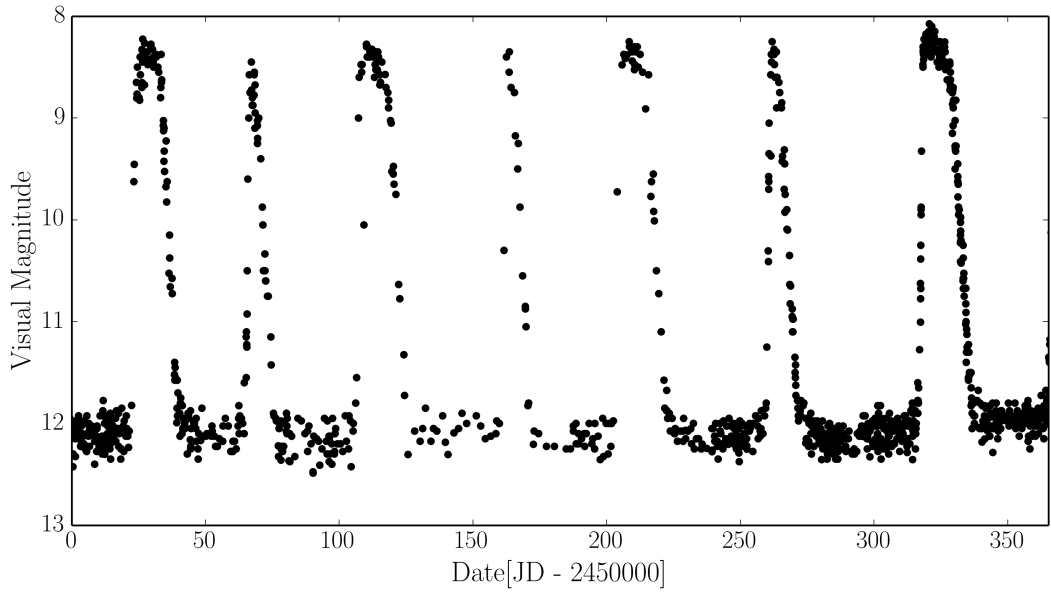


FIGURE 1.3: *Data: AAVSO.* A year in the life of SS Cyg, showing the characteristic repeated outbursts and periods of quiescence typical of a DN. SS Cyg has been undergoing this activity since it was first observed in 1896.

the stellar atmosphere disc spectrum computed in section 1.1.2.1, and to the intermediate inclination Nova-like variables discussed in the next section.

The leading candidate for explaining DN outbursts, and in fact the outbursts in low mass X-ray binaries or ‘soft X-ray transients’, is the disc-instability model (DIM; see [Lasota 2001](#), and references therin). In this model, a gradual increase in supply rate from the donor star (and hence surface density in the disc) causes the disc to heat up. Eventually, the disc hits a critical temperature, around 7000K, and becomes ionized. Now the surface density in the disc can increase significantly, and the disc becomes geometrically thin and optically thick. Most importantly, it can efficiently undergo radiative cooling, and a significant increase in brightness is observed.

1.2.2.2 Nova-like Variables

Nova-like variables (NLs) are similar to DNe in overall structure, except that the disc is always in a relatively high-accretion-rate state ($\dot{M} \sim 10^{-8} M_{\odot} \text{ yr}^{-1}$). NLs are therefore one of the best ‘laboratories’ for testing the steady-state accretion disc theory described in section 1.1.2.1. NLs generally exhibit a series of strong emission lines superposed on a blue continuum.

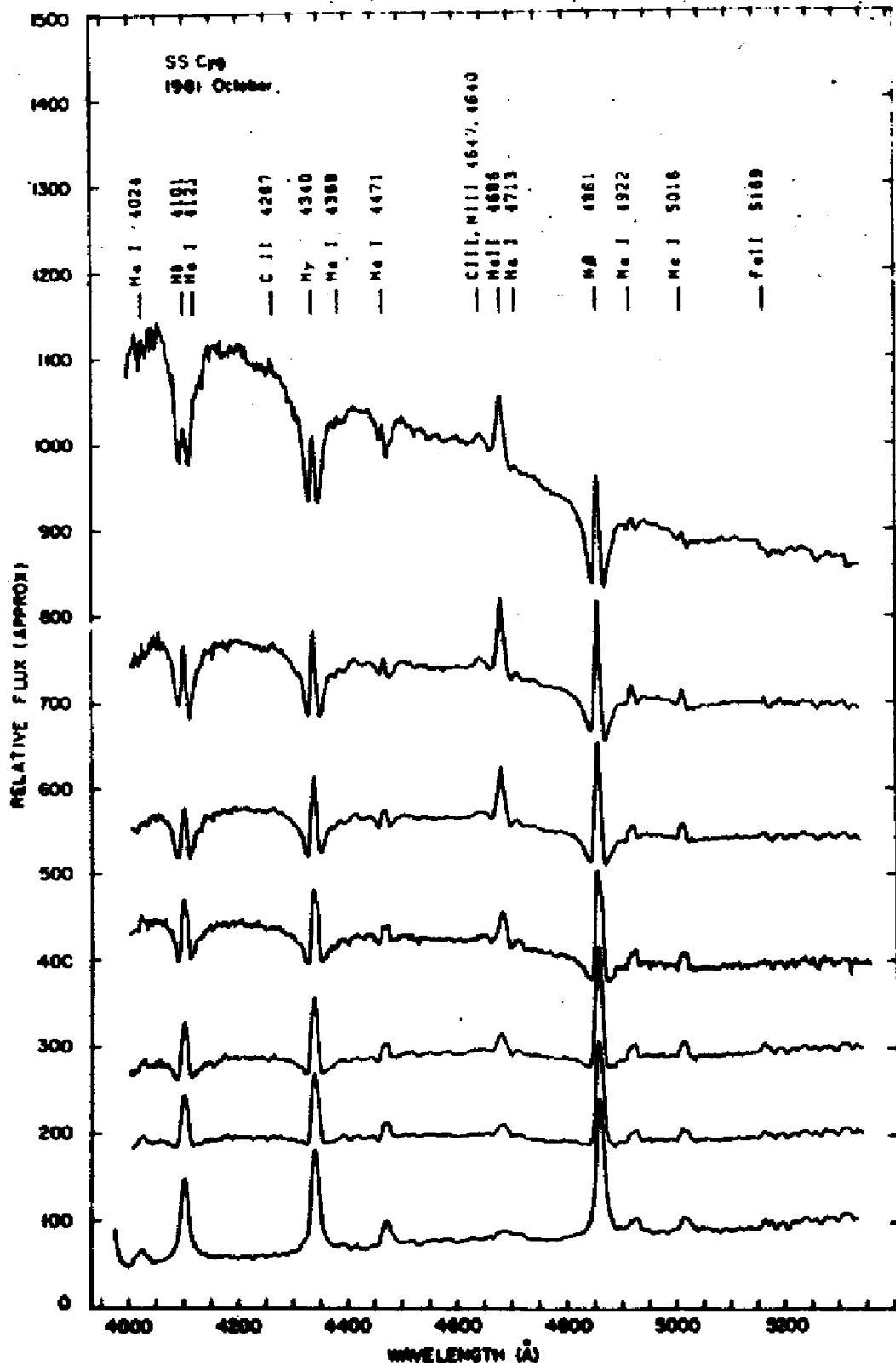


FIGURE 1.4: Credit: Hessman et al. 1984 / Dhillon et al. 1996. Spectra of SS Cyg during an outburst cycle, showing the evolution from minimum to maximum light. The rise is characterised by the appearance of an optically thick accretion disc spectrum. The flux scale is approximate.

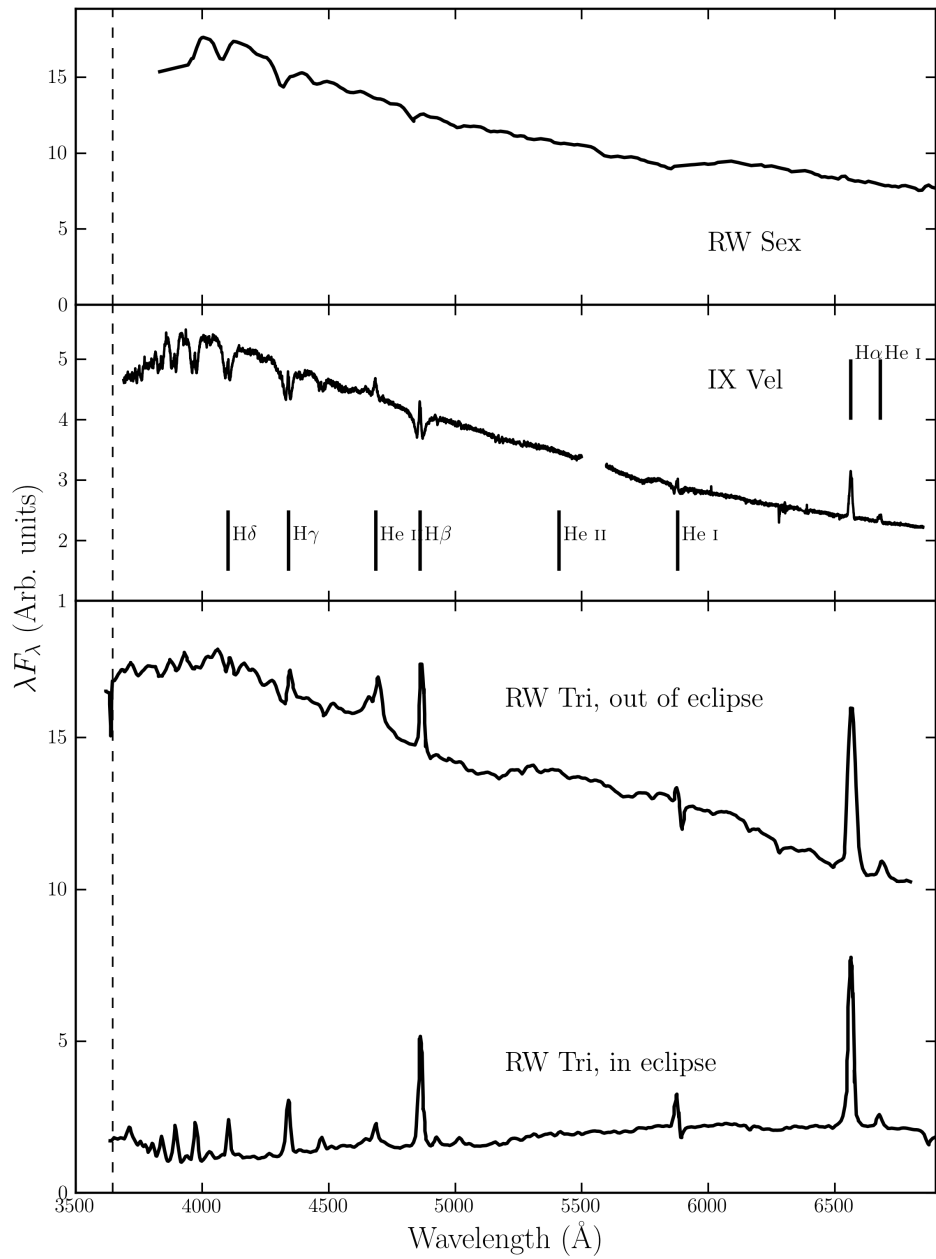


FIGURE 1.5: Optical spectra of three nova-like variables.

1.2.3 Low Mass X-ray Binaries

X-ray binaries are similar to CVs in structure, except that the compact object is either a neutron star (NS) or black hole (BH). The accretion disc emits in the soft X-rays, and an additional hard X-ray power law is also seen in the spectrum (REFs). This hard component is normally attributed to Compton up-scattering of seed disc photons by some kind of ‘corona’ of hot electrons close to the BH (REFs). A characteristic spectrum is shown in figure ??.

Although I do not discuss XRBs directly in this thesis, it is instructive to discuss some of their observational appearance as it is instructive for understanding the theory of disc winds, as well as their wider significance. The discovery that XRBs follow similar tracks on a hardness-intensity diagram (REFs) is particularly interesting in this regard, especially since Ponti et al. (2012) showed that broad Fe absorption lines are only seen in the soft-state high-inclination systems (see section 2.1.2). This implies that equatorial outflows are intrinsic to the accretion process. Although the driving mechanism is almost certainly different to CVs (Díaz Trigo and Boirin 2015), the similarity in general structure to models for CVs and quasars is striking.

1.3 Quasars and Active Galactic Nuclei

Spectra of AGN have now been studied for over 100 years, and we have known that they exhibit strong, broad emission lines since the first spectrum was taken by Fath (1909). However, it wasn’t until the work of Seyfert (1943) that the systematic classification of AGN really began, leading to the phrase ‘Seyfert galaxy’. This label was applied to galaxies possessing a bright nucleus, spectroscopically characterised by a blue continuum and a series of strong emission lines. The first real physical insight into the extraordinary nature of AGN was provided by Woltjer (1959), who noted that (i) the nuclei must have sizes < 100 pc, based on the fact that they were unresolved and (ii) the mass of the nucleus must be very high, based on virialised motion. While both of these observations were based on simple arguments, the fact that these ultra-luminous celestial objects are both *compact* and *supermassive* is perhaps the defining insight into the nature of AGN.

Although the field of AGN study was established in the optical, radio astronomy also significantly furthered our understanding of AGN in the mid-20th century. A number of surveys, such as the Cambridge (Edge et al. 1959), Parkes (Ekers 1969) and Ohio (Ehman et al. 1970) surveys discovered a great many bright radio point sources distributed isotropically across the sky. These sources eventually became known as ‘quasi-stellar radio sources’ or *quasars*, and were soon identified to be coincident with bright optical

sources or ‘quasi-stellar objects’ (QSOs; REFs). Nowadays, the term quasar normally has very little to do with radio emission and is often used interchangeably with QSO. Indeed, throughout this thesis I shall refer to a quasar as simply a bright, massive AGN; one with sufficiently high luminosity that it dominates the emission from its host galaxy.

1.3.1 AGN Taxonomy

In addition to Seyfert galaxies and quasars, there are a number of different classes of AGN. These are broadly characterised by their spectra in the optical, UV and X-ray as well as their radio behaviour. It is worth noting that these are observational classifications; that is, even after a century of study, the *physical* origins of the diverse behaviour of AGN are still an active area of research.

1.3.1.1 Radio Galaxies

Radio galaxies are a broad class of AGN, of which radio-loud quasars and blazars are technically members, which show strong emission in the radio band. The main classification scheme was proposed by [Fanaroff and Riley \(1974\)](#), who split sources according to the luminosity. FR I sources are lower in radio luminosity with a steadily decreasing surface brightness towards the edge of the radio lobes. FR II sources are more luminous and exhibit bright structures at the edge of their radio maps. Radio galaxies are not particularly relevant here, but it is worth noting that ‘Radio core dominance’, $\log R$, is often used as an orientation indicator ([Orr and Browne 1982](#); [Wills and Brotherton 1995](#)). This is because more pole-on sources should, in theory, be more dominated by their cores whereas edge-on sources should be more dominated by extended radio lobes. I discuss the use of orientation indicators further in chapter 6.

1.3.1.2 BL Lacs and Blazars

BL Lac objects – named for the first object of the class, BL Lacertae – are AGN with featureless non-thermal continua (see figure 1.6, and [Falomo et al. 2014](#), for a review), in contrast to Seyfert galaxies. Their optical flux is highly polarised ([Angel and Stockman 1980](#)) and they tend to exhibit large-scale optical variability, to the extent that they were originally classified as irregularly variable stars ([Hoffmeister 1929](#)). BL Lacs are a subset of a larger AGN class known as Blazars, the most luminous of which are known as optically violent variable (OVV) quasars ([Wright et al. 1998](#)). Blazars require relativistic beaming in order to explain their high radio luminosities ([Ghisellini et al. 1985, 1993](#)), implying that the jet is orientated towards the observer. These objects thus have an

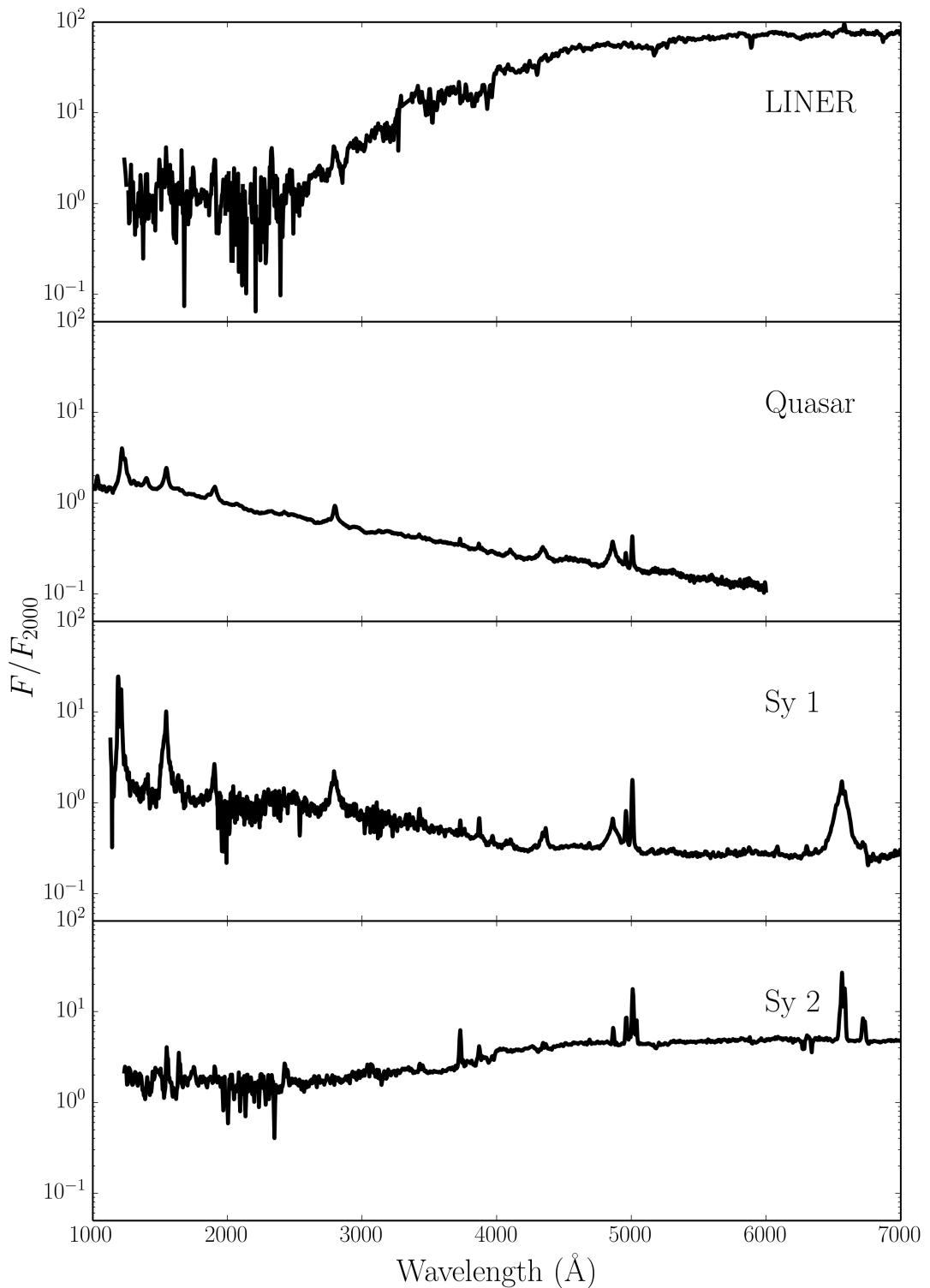


FIGURE 1.6: Template spectra, from the AGN atlas, for four common types of AGN.
Obtained from http://www.stsci.edu/hst/observatory/crds/cdbs_agn.html.

important place in unification schemes (see section 1.3.2), and allow us to measure bulk Lorentz factors in radio jets, which can be as high as ~ 50 (Begelman et al. 2008).

1.3.1.3 Obscured and Compton-thick AGN

1.3.1.4 Low-luminosity AGN

1.3.2 AGN Unification and the dusty Torus

Although Seyfert had identified type 1 and 2 AGN, a physical explanation for this dichotomy was not forthcoming until a study by (Antonucci and Miller 1985, AM85). They showed unambiguously that the nearby Seyfert 2 NGC 1068 is simply an obscured type 1 AGN, by finding that broad emission lines appeared in the spectrum of *polarised* flux. This provided the basis for the first successful attempt to unify AGN behaviour, as it elegantly explained the apparent disconnect between the two types of AGN as simply a viewing angle effect; at one angle, you could look directly into the broad line region (BLR) near the nucleus, but at Type 2 angles this region was hidden from view. The obscuring structure became known as the ‘torus’ (Krolik and Begelman 1986), due to its geometry, and it was soon realised that this structure may be made of dust, in which case it could also be responsible for the infra-red (IR) bump in AGN (Neugebauer et al. 1979).

(Urry and Padovani 1995, UP95) went further than the original unification model proposed by AM85 as they also tried to explain radio AGN phenomena. The picture they proposed is shown in figure 1.7. This model attempts to explain all of the types of AGN described in section 1.3.1 merely as a function of viewing angle and presence, or lack thereof, of a radio jet. Models such as this also describe the series of ‘bumps’ observed in AGN – the portions of the spectrum that dominate the luminosity, shown in figure 1.8. In most models, the ‘Big Blue Bump (BBB)’ is ascribed to thermal emission from an accretion disc, and the ‘Small Blue Bump’ to optically thin Balmer continuum and Fe II emission from the BLR. This can just be seen between $\sim 2000\text{\AA}$ and $\sim 4000\text{\AA}$ in the Seyfert 1 and quasar templates in figure 1.6 Our understanding of the BBB is still unsatisfactory (see section 1.4).

Since the seminal works by AM85 and UP95, the picture has become somewhat more complicated. Variable X-ray absorption has been detected in so-called ‘Changing look’ AGN (Matt et al. 2003; Puccetti et al. 2007), even in NGC 1068 itself (Marinucci et al. 2016). Changes in type have also been seen in the optical lines; the broad H β component can dramatically disappear or reappear (e.g. Tohline and Osterbrock 1976; Cohen et al. 1986; Denney et al. 2014). The explanation for this could be variable absorption (Elitzur

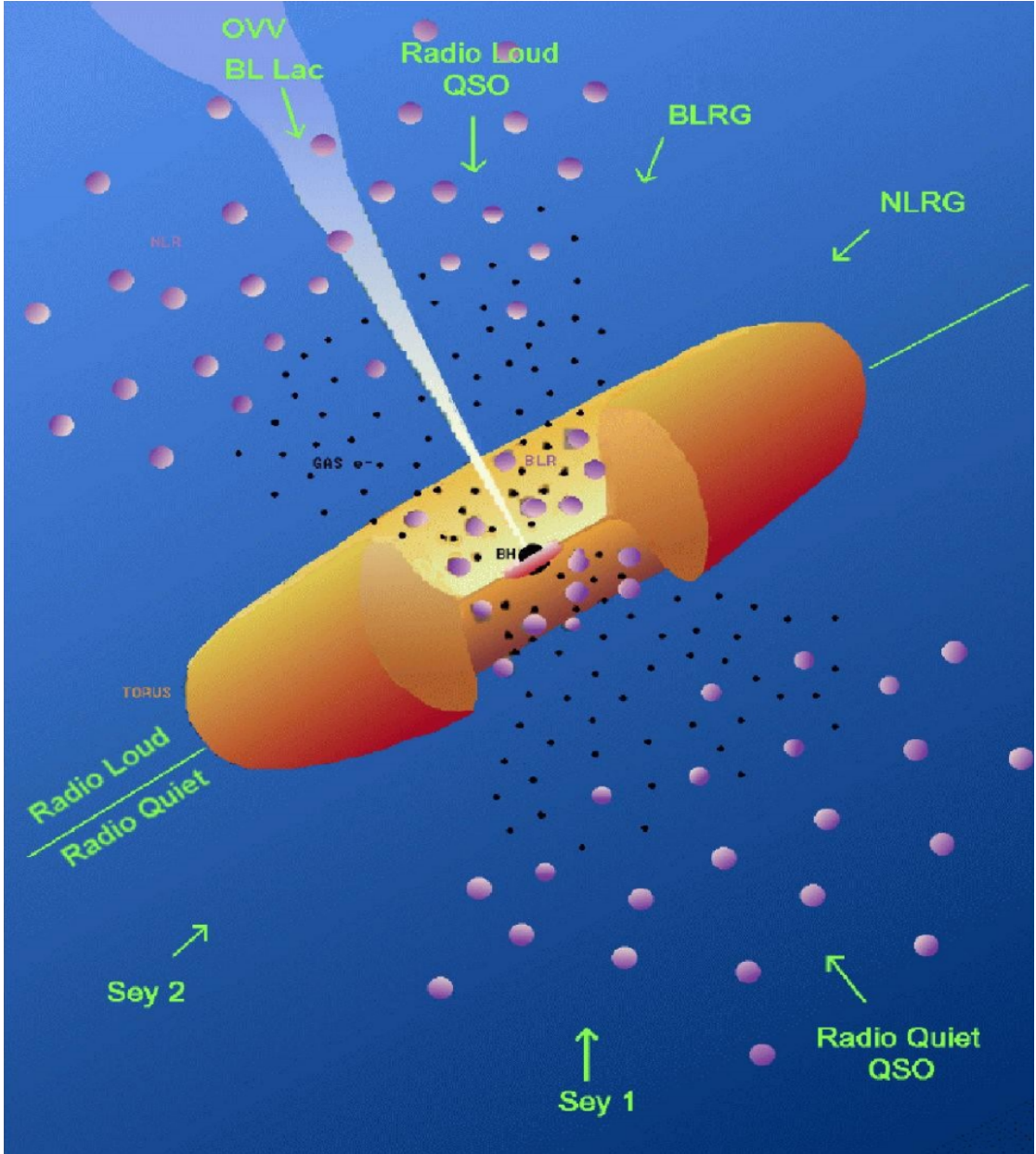


FIGURE 1.7: A unified scheme for AGN.

2012) or linked to the accretion state of the disc. In the latter case, it has even been suggested that a disc wind could be directly responsible for this change in accretion state (Elitzur et al. 2014). Furthermore, dusty *polar* outflows have been found to be important IR emitters (Hönig et al. 2013), implying that, even when it comes to dust, the torus is not the whole picture. Despite these complications, the AGN torus unification picture still helps explain a lot of AGN behaviour, and represents a good framework to test with observations.

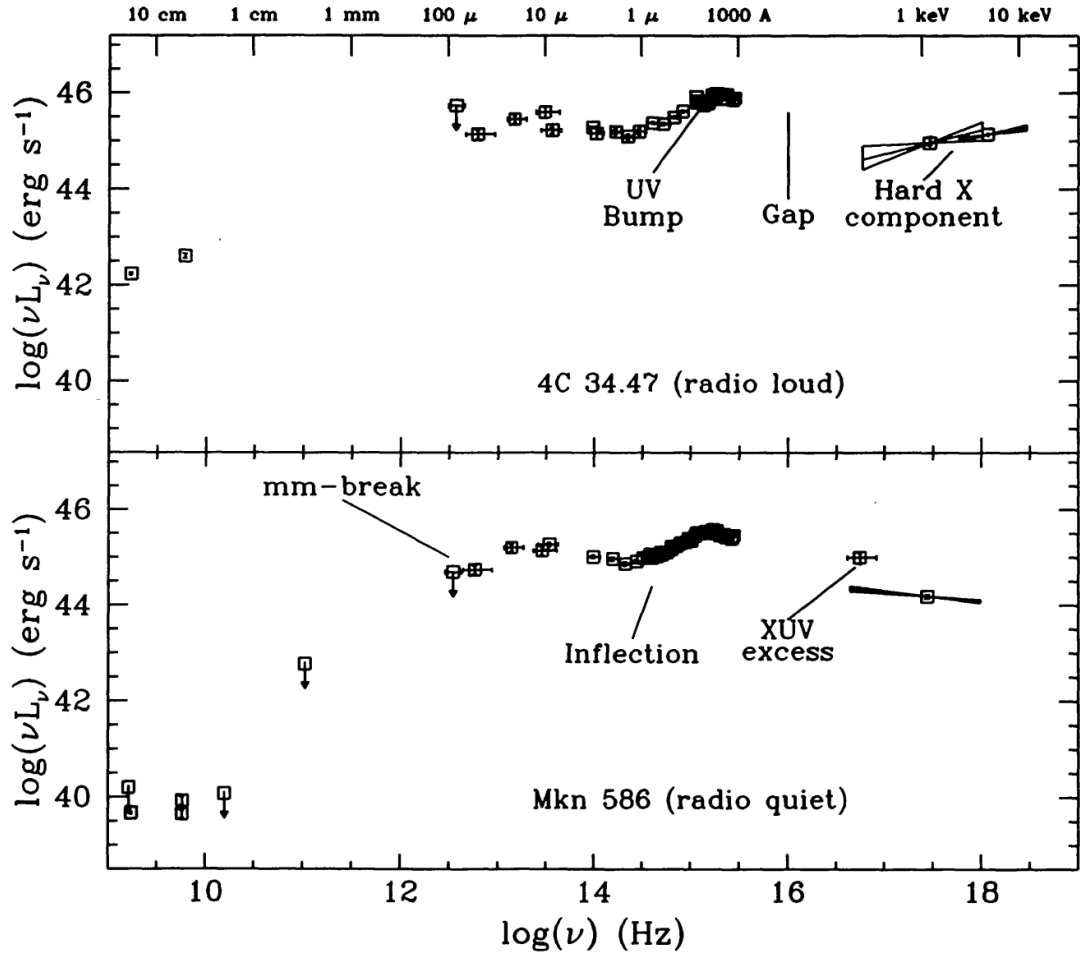


FIGURE 1.8: Radio-loud (top) and radio-quiet (bottom) quasar SEDs from Elvis (1994). The UV bump is the BBB, and the IR bump can clearly be seen. The XUV or Soft-X-ray excess is also visible in the radio-quiet panel (see section 1.4.2.4).

1.3.3 X-ray Properties of AGN

1.3.4 The Broad Line Region and Connection to Outflows

In the UP95 unification model, the broad emission lines come from a series of virialised clouds close to the disc plane. As noted by (Murray et al. 1995, hereafter MCGV95), there are a number of problems with the BLR ‘cloud’ model, perhaps most notably that there is no obvious physical origin for a series of virialised clouds. Testing alternative models for the BLR is therefore important. Indeed, MCGV95 proposed a disc wind model in order to explain both BALs and BELs in quasars. A disc wind model was also discussed by Elvis (2000), who proposed a structure for quasars that attempted to explain much of the behaviour of luminous AGN merely as a function of viewing angle. Outflow models are discussed further in section 2. The philosophy of these models is that, before invoking additional degrees of freedom in a model, we should first test if

OCCAM'S QUASAR: THE PRINCIPLE THAT IN EXPLAINING A QUASAR NO MORE ASSUMPTIONS SHOULD BE MADE THAN ARE NECESSARY.

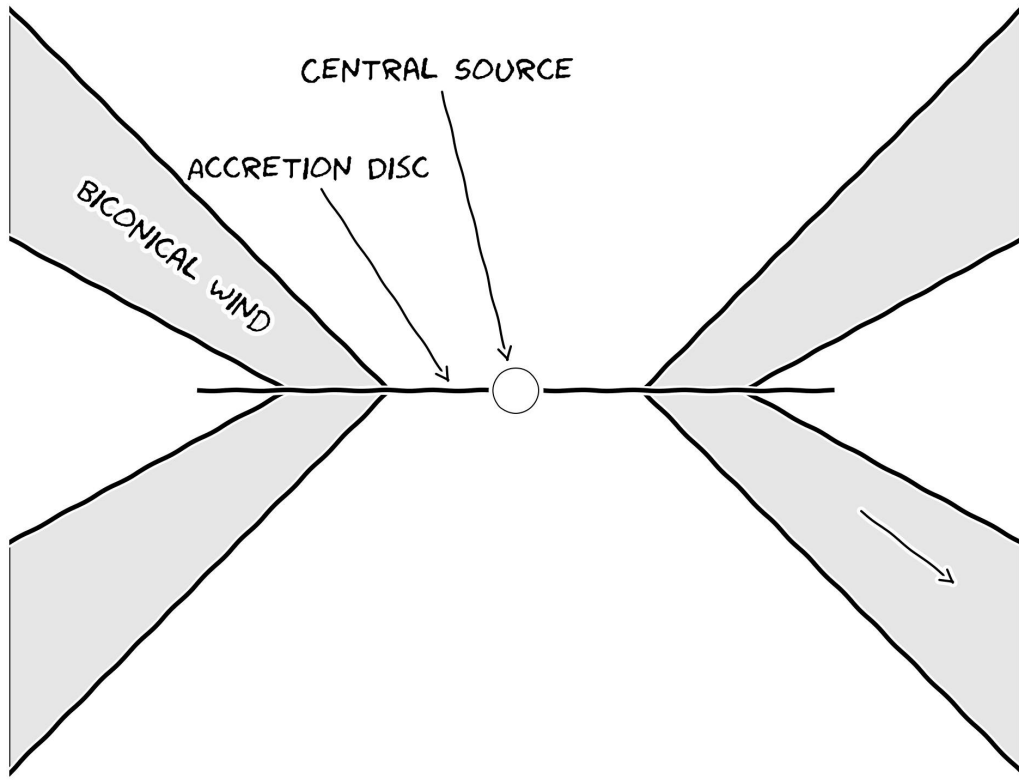


FIGURE 1.9: Occam's quasar. How far can this general picture take us when trying to explain the behaviour of quasars and other accreting compact objects?

known quasar phenomenology (winds) can explain other aspects of their observational appearance. I have illustrated this general principle with the ‘Occam’s quasar’ cartoon shown in figure 1.9. This is the picture that I will quantitatively test in the latter, quasar-focused sections of this thesis, and the general principle can even be applied to cataclysmic variables and other accreting objects.

1.4 The Current Understanding of the Disc Continuum

The SS73 model is still the most common way to fit accretion disc spectra and infer information about the underlying physics. However, a number of issues have been raised with the thin-disc model and its applicability to accreting systems.

1.4.1 The Spectral shape of CV discs

Attempts to fit the observed SEDs of high-state CVs with simple disc models have met with mixed success. In particular, the SEDs predicted by most stellar/disc atmosphere models are too blue in the UV (Wade 1988; Long et al. 1991, 1994; Knigge et al. 1998a) and exhibit stronger-than-observed Balmer jumps in absorption (Wade 1984; Haug 1987; La Dous 1989; Knigge et al. 1998a). One possible explanation for these problems is that these models fail to capture all of the relevant physics. Indeed, it has been argued that a self-consistent treatment can produce better agreement with observational data (e.g. Shaviv et al. 1991; but see also Idan et al. 2010). However, an alternative explanation, suggested by Knigge et al. (1998b; see also Hassall et al. 1985), is that recombination continuum emission from the base of the disc wind might fill in the disc's Balmer absorption edge and flatten the UV spectrum.

Alternatively, it may just be that CV disks are never really in a steady state, and so we should only expect the $R^{-3/4}$ temperature profile to hold in a limited portion of the disc. From eclipse mapping, it has been shown that the inferred accretion rate increases with radius in NLs (Rutten et al. 1992; Horne 1993). These results suggest that a non-radiative form of energy loss is present in the inner regions of the disc, of which potential forms would be advection or mass loss. This is yet another piece of evidence that the understanding of accretion and outflow are intertwined, although hopefully not inextricably.

1.4.2 The Big Blue Bump in AGN

1.4.2.1 Fitting AGN Spectra

1.4.2.2 The 1000Å Break

1.4.2.3 The Accretion Disc Size Problem

One of the most interesting results of recent years relating to AGN and accretion discs is the discovery that the continuum emission region size is a factor ~ 3 larger than predicted by standard Shakura & Sunyaev disc theory. This result has been found independently in both microlensing (Morgan et al. 2010) and reverberation (Edelson et al. 2015), and poses a challenge to the current best-fit model for the big blue bump in AGN. One proposed solution is that the discs in AGN are inhomogeneous, consisting of individual clumps with independently varying temperatures (Dexter and Agol 2011).

1.4.2.4 The Soft-Xray Excess

1.5 The Universality of Accretion

Accretion appears to be an important physical processes across ~ 10 orders of magnitude in mass. But is this process the same at all scales? Does any behaviour manifest in all accretion systems?

1.5.1 The RMS-flux relation

Broad-band variability is common in all types of accretion disc. It has been known for some time that there exists a linear relationship between the flux and absolute root-mean-square (rms) amplitude of this variability. This was discovered first in XRBs and AGN ([Uttley and McHardy 2001](#); [Uttley et al. 2005](#); [Heil et al. 2012](#)), but it has been shown more recently that the relationship extends to CVs and even YSOs ([Scaringi et al. 2012, 2015](#)). The relationship is not limited to one type of CV, as it is present in both NLs and DNe ([Van de Sande et al. 2015](#)).

The model that best reproduces this behaviour is the so-called ‘fluctuating accretion disc’ model ([Lyubarskii 1997](#); [Kotov et al. 2001](#); [Arévalo and Uttley 2006](#); [Hogg and Reynolds 2015](#)). It has been shown that additive processes cannot reproduce the behaviour, and a multiplicative mechanism is required ([Uttley et al. 2005](#)). Regardless of the mechanism, the rms-flux relation is one of the most clear-cut examples of a universal accretion phenomenon. It tells us that at least some of the behaviour in CV discs is present in AGN and XRBs, strengthening the argument that CVs should be used as ‘accretion laboratories’.

1.5.2 Accretion States

1.5.3 Jets and Outflows

1.5.4 A Global Picture

Clearly, accretion physics is relevant to a plethora of astrophysical phenomena. It would also appear that the outflowing material observed in accreting systems has a profound effect on the accretion process itself, as well as acting as a spectral ‘filter’ – modifying, and sometimes dominating the observational appearance of accretion discs.

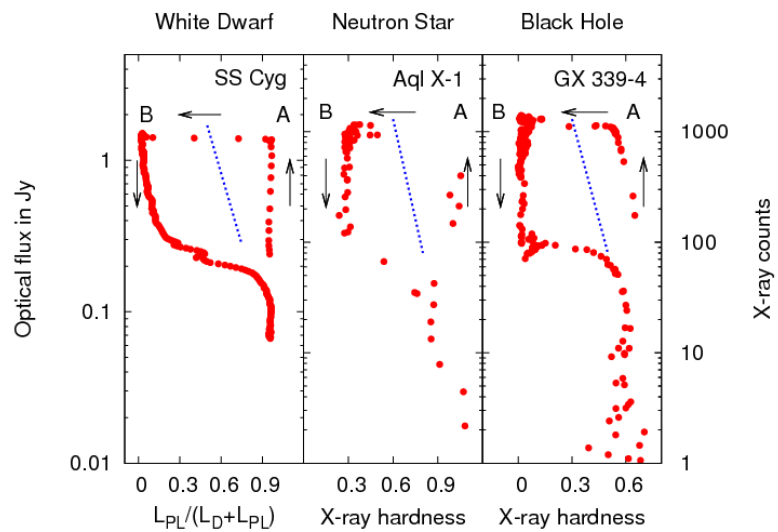


FIGURE 1.10: Credit: Kording et al. XXXX. Caption.

Chapter 2

Accretion Disc Winds

“A view of space, with an elephant
obstructing it”

Mike Vennart, Silent/Transparent

2.1 Accretion Disc Winds: Observational Evidence

2.1.1 Cataclysmic Variables

2.1.2 X-ray Binaries

2.1.3 AGN and Quasars

2.1.3.1 Broad Absorption Line Quasars

2.1.3.2 Warm Absorbers

2.1.3.3 Ultra-fast Outflows

2.1.4 Stellar Winds

2.1.4.1 Clumping

2.2 Accretion Disc Winds: Driving Mechanisms

Let us consider a parcel of ideal gas. By imposing nothing more than conservation of mass, energy and momentum on that parcel we can write down three equations of

hydrodynamics ¹

$$\frac{D\rho}{Dt} + \rho \nabla \cdot \vec{v} = 0 \quad (2.1)$$

$$\rho \frac{Dv}{Dt} = -\nabla P + \frac{1}{4\pi} (\nabla \times \vec{B}) \times \vec{B} + \rho \vec{F}_{rad} + \rho \vec{g} \quad (2.2)$$

$$\rho \frac{D}{Dt} \left(\frac{e}{\rho} \right) = P \nabla \cdot \vec{v} + \rho \mathcal{L} \quad (2.3)$$

Here D denotes a derivative within the comoving frame of the gas parcel, \vec{v} is the velocity, ρ is the gas density, \vec{B} is the local magnetic field, \vec{F}_{rad} is the radiation force per unit mass and \vec{g} denotes the gravitational acceleration vector. Equation 2.1 is the *continuity equation* and describes conservation of mass. Equation 2.2 is the *equation of motion* and describes conservation of momentum. Equation 2.3 is the *equation of energy conservation*. We can use equation 2.2 to neatly demonstrate how an outflow can be driven. I have deliberately written the equation so that all the force terms lie on the RHS. We can then see that for an outflow to be driven from an accreting object one simply needs one of the terms on the RHS to dominate over gravity, $\rho \vec{g}$. These terms thus signify three potential driving mechanisms.

- Magnetic Forces, $\frac{1}{4\pi} (\nabla \times \vec{B}) \times \vec{B}$.
- Radiative Forces, $\rho \vec{F}_{rad}$.
- Thermal Pressure, $-\nabla P$.

We can now examine under what physical conditions (and in which corresponding astrophysical objects) we might expect these forces to overcome gravity and cause a parcel of mass to escape to infinity. In other words: *what might drive a wind?*

2.2.1 Thermal Winds

In hydrostatic equilibrium (HSE), thermal pressure balances gravity and no other forces are present, meaning that the equation of motion can be written as

$$\rho \frac{Dv}{Dt} = -\nabla P + \rho \vec{g} = 0 \quad (2.4)$$

¹I stress that these equations are not used in hydrodynamic simulations in this thesis (see section ?, for example); they are discussed here because they provide a natural reference point for exploring potential driving mechanisms for winds in accreting systems.

Clearly, if the thermal pressure is then significantly increased then this equilibrium condition no longer holds. This can occur in accretion discs at temperatures in excess of $\sim 10^7$ K – where other forces are negligible compared to thermal pressure – and where the escape velocities are relatively low (i.e. far out in the disc). Due to the temperature and gravity scalings, this means that XRBs are natural candidates for showing evidence of thermally driven winds. The outer disc can be heated to the Compton temperature by the central X-ray source, potentially driving relatively high mass-loss rate outflows ([Begelman et al. 1983](#); [Woods et al. 1996](#)). This driving mechanism has been proposed as a natural explanation for the ever-present equatorial outflows in soft state XRBs ([Ponti et al. 2012](#)). However, they are much less likely candidates in CVs and AGN **Discuss scaling arguments with equations?**.

2.2.2 Radiatively Driven Winds

2.2.3 Line-driven Winds

2.2.4 Magneto-centrifugal Winds

2.3 Accretion Disc Wind Models

2.4 A Kinematic Prescription

2.5 The really, really big picture: AGN Feedback

The event horizon of a $10^9 M_\odot$ BH is approximately 10^{15} cm, a billionth of the size of a typical galactic bulge. This is roughly the difference in size between a small coin and the radius of the Earth. Despite this vast different in scale, there are multiple pieces of evidence that the physics on the scale of the gravitational radius of the BH really does affect the evolution and dynamics of its host galaxy. I shall briefly discuss the evidence for this statement, and assess the potential role of winds together with alternative mechanisms.

2.5.1 Observational evidence for feedback

Perhaps the most famous pieces of evidence for some kind of long-distance relationship between a central BH and its host galaxy are the $M_{BH} - \sigma_*$ and $M_{BH} - M_{bulge}$ correlations, shown in figures ?? and [2.2](#) respectively.

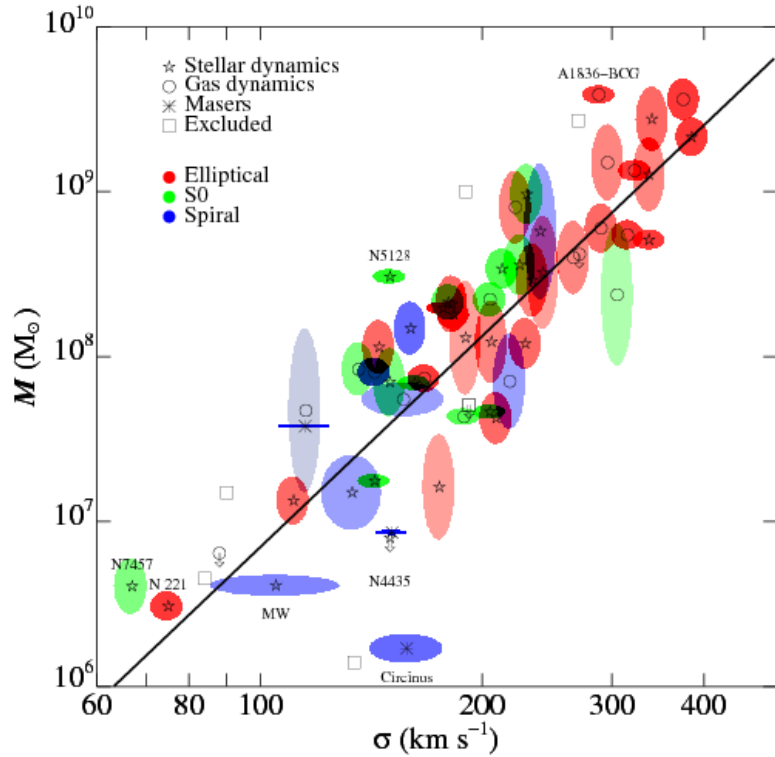


FIGURE 2.1: Credit: Gultekin et al. 2009. The $M_{BH} - \sigma_*$ correlation.

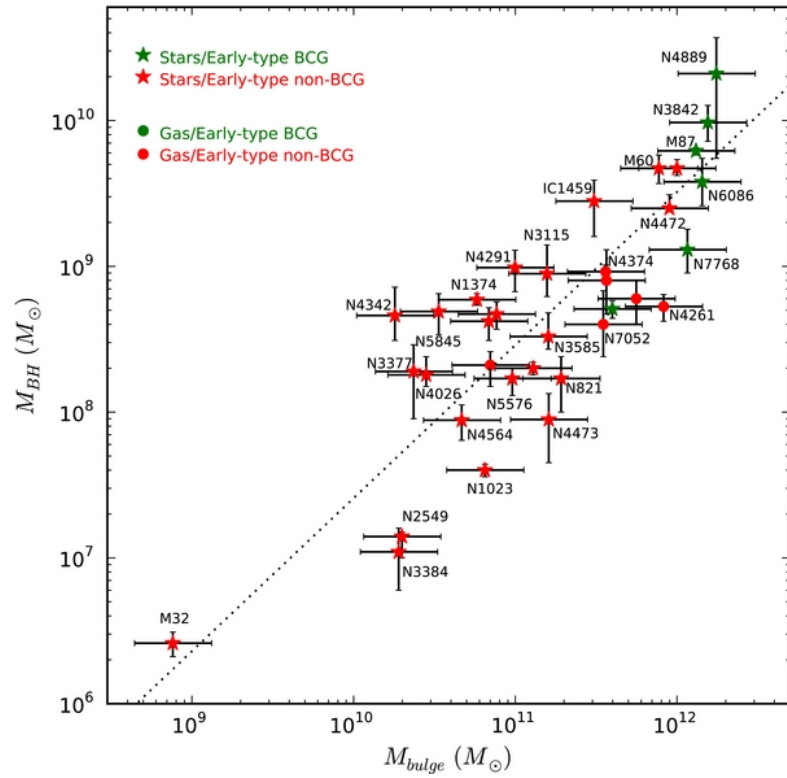


FIGURE 2.2: Credit: McConnell & Ma 2013. The $M_{BH} - M_{bulge}$ correlation.

2.5.2 Radiative or quasar mode feedback

2.5.3 Kinetic or radio mode feedback

2.5.4 In-situ Explanations

Chapter 3

Radiative Transfer and Ionization

“I’m splashing greys where once was
glowing white”

Mike Vennart, Silent/Transparent

In the previous chapters I have given an introduction to the field and some relevant background relating to accretion discs and their associated outflows. Now it proves useful to discuss some of the specific *methods* one might be able to use in order to answer some of the questions raised in the previous sections. In particular, I will discuss radiative transfer techniques and their potential applications.

3.1 Fundamentals of Radiative Transfer

The most fundamental quantity of radiative transfer is the *specific intensity*, I_ν , defined as

$$I_\nu = \frac{dE}{d\Omega dt dA d\nu}, \quad (3.1)$$

which has units of $\text{erg s}^{-1} \text{ Hz}^{-1} \text{ sr}^{-1} \text{ cm}^{-2}$. By successively multiplying by $\cos \theta$ and integrating over solid angle we can obtain the first and second ‘moments’ of the radiation field. These are the flux, F_ν and momentum flux, p_ν , respectively, given by

$$F_\nu = \int I_\nu \cos \theta d\Omega, \quad (3.2)$$

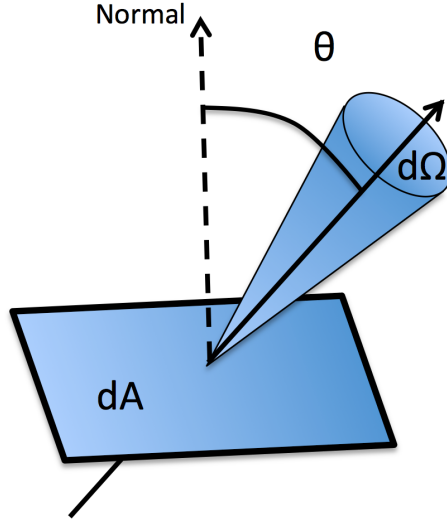


FIGURE 3.1: A schematic showing a ray obliquely incident on a surface of area dA . The labeled quantities are used in the definition of specific intensity.

$$p_\nu = \frac{1}{c} \int I_\nu \cos^2 \theta \, d\Omega \quad (3.3)$$

We can also define the *mean intensity*, J_ν , as

$$J_\nu = \frac{1}{4\pi} \int I_\nu \, d\Omega \quad (3.4)$$

The mean intensity is particularly useful when one wants to ignore the solid angle dependence of the radiation, for example when considering the impact of an ionizing radiation field.

The equation describing the specific intensity change along a path element ds is the radiative transfer equation,

$$\frac{dI_\nu}{ds} = -\kappa_\nu I_\nu + j_\nu, \quad (3.5)$$

where κ_ν and j_ν are the absorption and emission coefficients respectively. If we define the optical depth $d\tau_\nu = \kappa_\nu ds$ we can recast this as

$$\frac{dI_\nu}{d\tau_\nu} = -I_\nu + S_\nu \quad (3.6)$$

where $S_\nu = j_\nu / \kappa_\nu$ is the source function. This equation is called the *formal radiative transfer equation*, and can be solved to give

$$I_\nu = I_{\nu,0} e^{-\tau_\nu} + \int_0^{\tau_\nu} S_\nu(\tau'_\nu) e^{\tau'_\nu - \tau_\nu} d\tau'_\nu. \quad (3.7)$$

A useful limit is when the source function is constant in the absorbing medium, in which case the integral can be easily evaluated to give

$$I_\nu = I_{\nu,0} e^{-\tau_\nu} + S_\nu(1 - e^{-\tau_\nu}). \quad (3.8)$$

3.1.1 Spectral Line Formation

From the above equations, it is trivial to show how emission and absorption lines form when the source function is approximately constant. Say we have a plasma illuminated by a blackbody of temperature T_0 , such that $I_{\nu,0} = B_\nu(T_0)$. The plasma layer then has a different temperature, T , such that $S_\nu = B_\nu(T)$ in that medium. By inspecting equation 3.8 we can see that if we are optically thick within the line, but optically thin in the continuum, then inside the line the source term is dominant and outside the line the first $I_{\nu,0} e^{-\tau_\nu}$ term dominates. Therefore, if $T > T_0$ we will see an emission line, and if $T < T_0$ we will see an absorption line. This approach describes line emission in the blackbody limit; for more complicated SED shapes it is necessary to construct simple model atoms.

3.1.2 The Two Level Atom

The two level atom formalism is well described by Mihalas (1978).

3.1.2.1 Einstein Coefficients

Within the two level atom, the rate equation between the two levels in LTE can be written by invoking detailed balance, such that

$$B_{lu}\bar{J}_{ul}n_l = B_{ul}\bar{J}_{ul}n_u + A_{ul}n_u, \quad (3.9)$$

where B_{ul} , B_{2ul} and A_{ul} are the *Einstein coefficients* for absorption, stimulated emission and spontaneous emission respectively. The ‘mean intensity in the line’, \bar{J}_{ul} , is given by

$$\bar{J}_{ul} = \int \phi(\nu) J_\nu d\nu. \quad (3.10)$$

In LTE, the level populations obey Boltzmann statistics, and thus we can also write

$$\frac{n_l}{n_u} = \frac{g_l}{g_u} \exp(h\nu_{ul}/k_B T) \quad (3.11)$$

We can then rearrange equation 3.9 in terms of the mean intensity, and use the fact that, in LTE, $\bar{J}_{ul} = B_\nu(T)$ to write

$$\bar{J}_{ul} = (2h\nu_{ul}^3)/c^2. \quad (3.12)$$

Since this must be true at all values of T we can also show that

$$A_{ul}/B_{ul} = (2h\nu_{ul}^3) \quad B_{lu}/B_{ul} = g_u/g_l \quad (3.13)$$

3.1.2.2 Collision Strengths

As well as radiative excitation and de-excitation, bound electrons can also interact with the thermal pool of free electrons, meaning that collisional rates also affect

3.1.3 The Sobolev Approximation

The Sobolev approximation (SA) is a useful limit originally developed. It is used to treat line transfer in fast-moving flows. Originally the theory was mostly applied to Stellar winds, although since then a wide variety of astrophysical objects have been modelled using Sobolev treatments, such as accreting systems (this work) and Supernovae.

The Sobolev limit is when the local bulk velocity gradients in a flow dominate other any thermal broadening. In the presence of these steep velocity gradients, one can assume that the interaction of a ray with a bound-bound transition takes place over a small resonant zone, known as a ‘Sobolev surface’. The length of this zone is defined by

$$l_s = \frac{v_{th}}{dv/ds}. \quad (3.14)$$

It is important that the physical conditions of the c do not change on this scale. If this is the case, then we can assume that all line interactions for a given frequency will occur at a single ‘resonant’ point. The location at which a given photon will interact with a line of frequency ν_{lu} is then given, in velocity space, by

$$v = c \left(\frac{\nu}{\nu_{lu}} + 1 \right). \quad (3.15)$$

The Sobolev optical depth is then

$$d\tau = \frac{\pi e^2}{mc} \left(n_l - n_u \frac{g_l}{g_u} \right) \frac{f_{lu} \lambda_{lu}}{c|dv/ds|}. \quad (3.16)$$

We can see that the physical quantities determining line opacity are therefore the level populations in the plasma, the velocity gradient and the atomic physics associated with the bound-bound transition.

3.1.3.1 Escape Probabilities

3.1.4 Monte Carlo approaches

Simple radiation transfer problems can be solved analytically, but with more complicated geometries it is necessary to use Monte Carlo techniques, which are easily solved with modern computing approaches and are intuitively parallelisable problems. I will describe one specific Monte Carlo radiative transfer (MCRT) code, which has been used for the majority of the work in this thesis.

3.2 PYTHON: A Monte Carlo Ionization and Radiative Transfer Code

PYTHON¹ is a Monte Carlo ionization and radiative transfer code. The code has already been described extensively by LK02, SDL05 and Higginbottom et al. (2013; hereafter H13), so here we provide only a brief summary of its operation, focusing particularly on new aspects of our implementation of macro-atoms into the code.

3.2.1 Basics

PYTHON operates in three distinct stages, shown in figure 3.2. First, the user specifies the photon sources, geometry and kinematics of the system, normally with a similar parameterisation to the SV93 model described in section ???. The outflow is then discretised into a logarithmic grid with a user-specified resolution, and the density and velocity in each cell is calculated.

Once the basic setup process has been carried out, the ionization state, level populations and temperature structure are calculated. This is done via an iterative process, by

¹Named c. 1995, predating the inexorable rise of a certain widely used programming language.

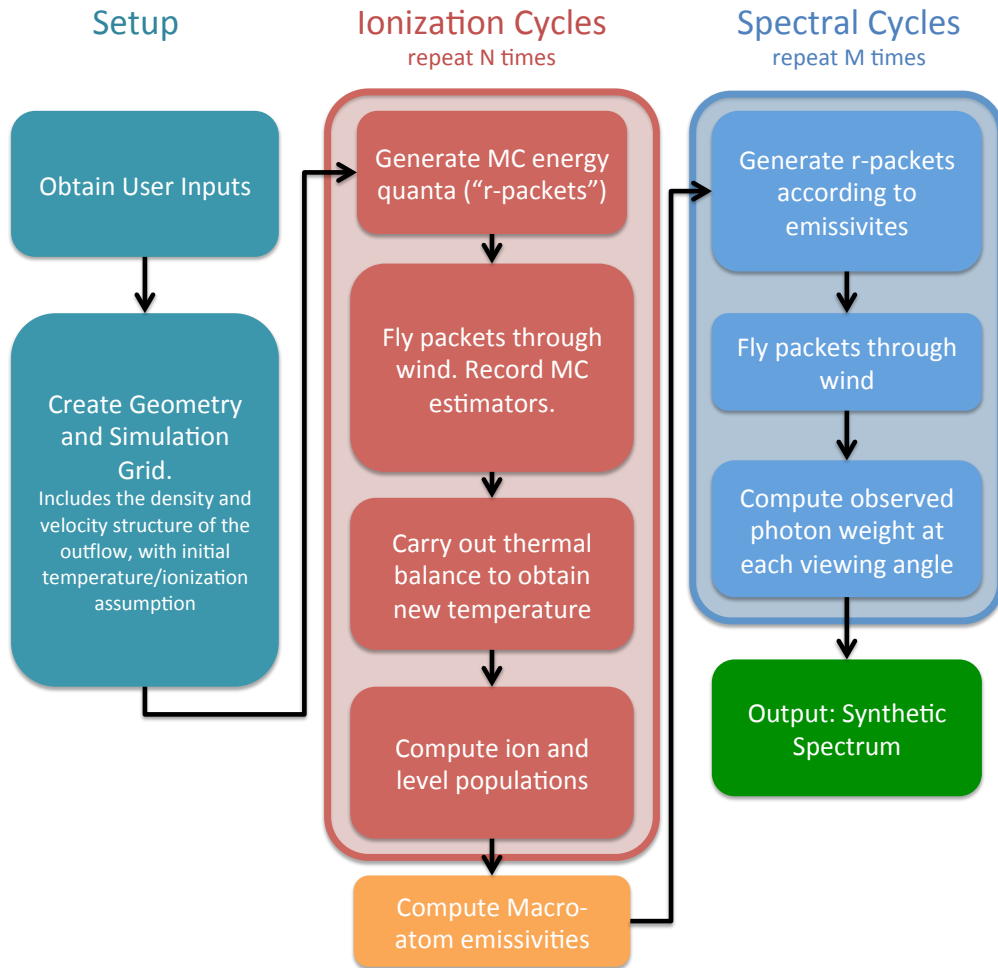


FIGURE 3.2: A flowchart showing the basic operation of PYTHON.

transporting several populations of Monte Carlo energy quanta ('photons' or 'r-packets) through the outflow. This process is repeated until the code converges. In each of these iterations ('ionization cycles'), the code records estimators that characterize the radiation field in each grid cell. At the end of each ionization cycle, a new electron temperature is calculated that more closely balances heating and cooling in the plasma. The radiative estimators and updated electron temperature are then used to revise the ionization state of the wind, and a new ionization cycle is started. The process is repeated until heating and cooling are balanced throughout the wind.

This converged model as the basis for the second set of iterations ('spectral cycles'), in order to compute the synthetic spectrum based on the MC estimators record during the ionization cycles. The emergent spectrum over the desired spectral range is synthesized by tracking populations of energy packets through the wind and computing the emergent spectra at a number of user-specified viewing angles.

PYTHON is designed to operate in a number of different regimes, both in terms of the scale of the system and in terms of the characteristics of the underlying radiation field. It was originally developed by LK02 in order to model the UV spectra of CVs with a simple biconical disc wind model. SDL05 used the code to model Brackett and Pfund line profiles of H in young-stellar objects (YSOs). As part of this effort, they implemented a ‘macro-atom’ mode (see below) in order to correctly treat H recombination lines with PYTHON. Finally, H13 used PYTHON to model broad absorption line (BAL) QSOs. For this application, an improved treatment of ionization was implemented, so that the code is now capable of dealing with arbitrary photo-ionizing SEDs, including non-thermal and multi-component ones.

3.3 Macro-atoms

The macro-atom scheme was created by Leon Lucy and is outlined in his 2002/03 papers. It was implemented in PYTHON by Stuart Sim, initially for the study of recombination lines in YSO (Sim et al. 2005).

Lucy (2002, 2003; hereafter L02, L03) has shown that it is possible to calculate the emissivity of a gas in statistical equilibrium without approximation for problems with large departures from LTE. His macro-atom scheme allows for all possible transition paths from a given level, dispending with the two-level approximation, and provides a full non-local thermodynamic equilibrium (NLTE) solution for the level populations based on Monte Carlo estimators. The macro-atom technique has already been used to model Wolf-Rayet star winds (Sim 2004), AGN disc winds (Sim et al. 2008; Tatum et al. 2012), supernovae (Kromer and Sim 2009; Kerzendorf and Sim 2014) and YSOs (SDL05). A full description of the approach can be found in L02 and L03.

The fundamental approach here requires somewhat of a philosophical shift. Normally MCRT is described in the most intuitive way- that is, we imagine real photons striking atoms and scattering, or photoionizing and depositing energy in a plasma. With Lucy’s scheme one should instead reimagine the MC quanta as a packets of quantised energy flow, and the scheme as a *statistical* one. The amount of time a given energy quanta spends in a specific atomic level or thermal pool is then somewhat analogous to the absolute energy contained therein.

Following L02, let us consider an atomic species interacting with a radiation field. If the quantity ϵ_j represents the ionization plus excitation energy of a level i then the rates at which the level j absorbs and emits radiant energy are given by

$$\dot{A}_j^R = R_{\ell j} \epsilon_{j\ell'} \quad \text{and} \quad \dot{E}_i^R = R_{j\ell'} \epsilon_{j\ell'} \quad , \quad (3.17)$$

Where we adopt Lucy's convention in which the subscript ℓ' denotes a summation over all lower states. Similarly, the rates corresponding to *kinetic* energy transport can then be written as

$$\dot{A}_j^C = C_{\ell' j} \epsilon_{j\ell'} \quad \text{and} \quad \dot{E}_j^C = C_{j\ell'} \epsilon_{j\ell'} \quad , \quad (3.18)$$

If we now impose statistical equilibrium

$$(\mathcal{R}_{\ell' j} - \mathcal{R}_{j\ell}) + (\mathcal{R}_{uj} - \mathcal{R}_{ju}) = 0 \quad . \quad (3.19)$$

we can then obtain

$$\begin{aligned} & \dot{E}_j^R + \dot{E}_j^C + \mathcal{R}_{ju} \epsilon_i + \mathcal{R}_{j\ell} \epsilon_\ell \\ &= \dot{A}_j^R + \dot{A}_j^C + \mathcal{R}_{uj} \epsilon_i + \mathcal{R}_{\ell j} \epsilon_\ell. \end{aligned} \quad (3.20)$$

This equation is the starting point for the macro-atom scheme. It shows that, when assuming only radiative equilibrium, the energy flows through a system depend only on the transition probabilities and atomic physics associated with the levels the energy flow interacts with. By quantising this energy flow into radiant (r-) and kinetic (k-) packets, we can simulate the energy transport through a plasma discretised into volume elements (“macro-atoms”), whose associated transition probabilities govern the interaction of radiant and kinetic energy with the ionization and excitation energy associated with the ions of the plasma.

Although equation 3.20 assumes strict radiative equilibrium, it is trivial to adjust it to include non-radiative source and sink terms. For example, in an expanding parcel of plasma, adiabatic cooling may be included with a simple modification to the RHS of equation 3.20.

3.3.1 Macro-Atom Estimators

3.3.1.1 Radiation Field Estimators

One of the most important estimators is the ‘mean intensity in the line’, \bar{J}_{lu} , which is defined by equation 3.10.

3.3.1.2 Heating And Cooling Estimators

3.3.2 Ionization Fractions and Level Populations

3.4 Simple-atoms

3.5 Heating And Cooling

3.5.1 Heating And Cooling Balance

3.5.2 Heating And Cooling Estimators

Here I’ve tried to use Lucy’s notation for macro-atom estimators. Take a three level system, in which l and u represent lower and upper levels, and κ represents the continuum level or upper ion. q is the ‘absorption fraction’ derived below, and q_{ul} and q_{lu} are the collisional rate coefficients.

3.5.2.1 Macro-atoms

In the macro-atom approach, we basically treat two communication pathways. bound-free transitions represent a way for radiant energy to communicate with the thermal pool and bound-bound transitions represent a way for excitation energy to communicate with the thermal pool.

The heating and cooling rates for macro-atom bound-bound transitions are the rates of collisional excitations and de-excitations - i.e. the rate at which thermal energy is converted into bound-bound excitation energy and vice versa.

$$C_{bb,matoms} = \sum_{lines} q_{lu} n_l n_e h \nu_{ul} V \quad (3.21)$$

$$H_{bb,matoms} = \sum_{lines} q_{ul} n_u n_e h\nu_{ul} V \quad (3.22)$$

For bound-free transitions, we define the normal photoionization and recombination rate coefficients γ and α , where α includes stimulated recombination as we do in the code. Note this differs to the approach in Lucy (2003), where it is instead included as a negative photoionization term, hence the notation $\tilde{\gamma}$. We also need to define two ‘modified rate coefficients’ which are the rates at which b-f transitions add and remove energy to the radiation field. These are denoted γ^E and α^E .

The rate at which recombinations convert thermal *and* ionization energy into radiant energy is then $\alpha^E h\nu_{kl} n_\kappa n_e$, where $h\nu_{kl}$ is the potential of the b-f transition, or the energy difference between continuum κ and the level l we are recombining too. The amount of this energy which is removed from the actual thermal pool therefore needs a quantity $\alpha h\nu_{kl} n_\kappa n_e$ subtracted from it, giving

$$C_{bf,matoms} = \sum_{bfjumps} (\alpha^E - \alpha) n_e n_\kappa \nu_{kl} V \quad (3.23)$$

where here I have also included stimulated recombination as we do in the code. Note this differs to the approach in Lucy (2003), where it is instead included as a negative photoionization term, hence the notation $\tilde{\gamma}$. For photoionizations, we write a similar expression. The rate of at which a level l absorbs energy by b-f transitions is given by $\gamma^E h\nu_{kl} n_\kappa n_e$, but the amount $\gamma h\nu_{kl} n_l$ goes into ionization energy, giving

$$H_{bf,matoms} = \sum_{bfjumps} (\gamma^E - \gamma) n_l h\nu_{kl} V \quad (3.24)$$

as the rate at which radiant energy heats the plasma via b-f transitions.

3.5.2.2 Simple-atoms

In simple-ions it is in some ways a little more complicated. First we define q which will be different for each b-b transition, following Nick’s thesis, which is given by (NB: I don’t actually know how to derive this)

$$q = \frac{q_{ul} n_e (1 - e^{-h\nu/kT_e})}{\beta_{ul} A_{ul} + q_{ul} n_e (1 - e^{-h\nu/kT_e})} \quad (3.25)$$

where β_{ul} is the angle-averaged escape probability. q represents *the probability that an excited bound electron will collisionally de-excite*. Our b-b heating rate is computed during the photon propagation and is a sum over photons which come into resonance

with each line, given by

$$H_{bb,simple} = \sum_{photons\ lines} \sum_{lines} (1-q)(1-e^{-\tau_S})w_{photon} \quad (3.26)$$

And our bound bound cooling rate is given by

$$C_{bb,simple} = \sum_{lines} q \left(n_l \frac{g_u}{g_l} - n_u \right) q_{ul} n_e \frac{(1-e^{-h\nu/kT_e})}{(e^{h\nu/kT_e} - 1)} h\nu_{ul} \quad (3.27)$$

The bound-free heating rate is given by

$$H_{bf,simple} = \sum_{photons\ bfjumps} \sum_{bfjumps} w_{photon} e^{-\tau} \frac{\nu - \nu_0}{\nu} \quad (3.28)$$

where ν here is the frequency of the photon in question, and ν_0 . The bound-free cooling rate is then

$$C_{bf,simple} = ?? \quad (3.29)$$

3.6 Spectral Synthesis

The primary output from PYTHON is a synthetic spectrum across a range of viewing angles. The code utilises a variance reduction technique in order to minimise the amount of time spent in the portion of the code. This technique is based on a similar method implemented by ([Woods 1991](#)).

A comparison between the two methods is shown in figure [3.3](#).

3.7 Atomic Data

One of the big challenges in building reliable photoionization and radiative transfer lies in the acquisition of accurate and complete atomic datasets. All of the rates described so far contain a term, such as the oscillator strength or dimensionless collision strength, that is dependent purely on the atomic physics associated with the transition. These quantities can be measured in laboratory experiments, or predicted from atomic structure codes which derive the atomic physics from quantum theory.

Photoionization cross-sections are obtained from two sources. Where possible, we use TOPBASE photoionization cross-sections. For macro-atoms, these cross-sections are

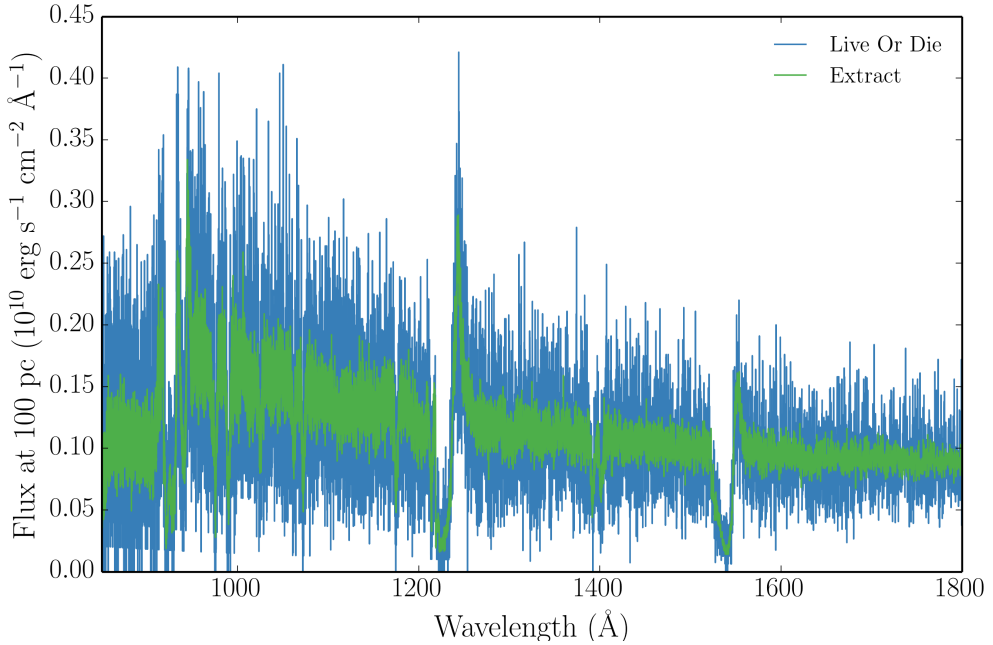


FIGURE 3.3: A Synthetic spectrum after 30 spectral cycles with 100,000 photons from simple CV wind model at a 60° viewing angle. Spectra produced with both the extract and live or die modes are shown. The effectiveness of the extract variance reduction technique can be clearly seen, and we can see that the spectral shape is unaltered.

partial and represent the cross-section for a photoionization from a given *level*. We neglect photoionizations to excited configurations of the upper ion. For simple-atoms they are from the ground state. The TOPBASE cross-sections have two major drawbacks in that

3.8 Clumping

3.8.1 Motivation

As described in section ??, observational evidence for inhomogeneities in outflows is widespread. Clumping a plasma can have a significant effect on its ionization, emission and absorption characteristics. Clearly, the interplay between these effects will be somewhat complex

A number of different implementations of clumping have been explored in previous studies, mostly in the stellar winds community. Perhaps the simplest method is when one assumes that the individual clumps are both optically and geometrically thin; this is known as *microclumping* (e.g. Hamann and Koesterke 1998; Hillier and Miller 1999;

[Hamann et al. 2008](#)). This technique has been particularly successful in reconciling discrepant mass-loss estimates. It was found that one would obtain different mass-loss rates depending on whether they were calculated from (i) UV resonance scattering of continuum photons (which scales linearly with density; a ‘ ρ -diagnostic’) or (ii) recombination and free-free emission process (which scale with the square of density; ‘ ρ^2 -diagnostics’). A clumped outflow would have enhanced densities in certain regions, and would thus mean that ρ^2 -diagnostics tend to overestimate the total mass-loss rates. Microclumping has helped verify this hypothesis with radiative transfer modelling (REFs). These clumpy models also provide better fits to the electron scattering wings of emission lines in stellar winds (?).

The second-generation of stellar wind codes went on step further by addressing the issue of *porosity*; that clumps will have a finite size, and thus gaps between the clumps may affect the emergent radiation field. This approach is known as *macroclumping*.

Describe macroclumping with references.

Implementing a treatment of clumping in accretion disc wind models is challenging, for two main reasons. First, the physical scale lengths and density contrasts in disc winds are not well-constrained from observations, especially in AGN. Second, there are significant computational difficulties associated with adequately resolving and realistically modelling a series of small scale, high density regions with a MCRT code. Given the lack of knowledge about the actual type of clumping, we incorporated the simpler microclumping approach into our code. This is partly because our primary concern was the ionization and emission characteristics of the flow, and porosity was a secondary concern.

3.8.2 Microclumping

To take account of clumping in our outflow we adopt a simple parameterization used in stellar wind modelling. The key assumption here is that typical clump sizes are much smaller than the typical photon mean free path, and thus the clumps are both geometrically and optically thin. This approach is typically known as microclumping and allows one to introduce a ‘filling factor’, f , which is the fraction of the volume of the plasma filled by clumps. We can then introduce the ‘density enhancement’, D , which is simply

$$D = \frac{1}{f} \quad (3.30)$$

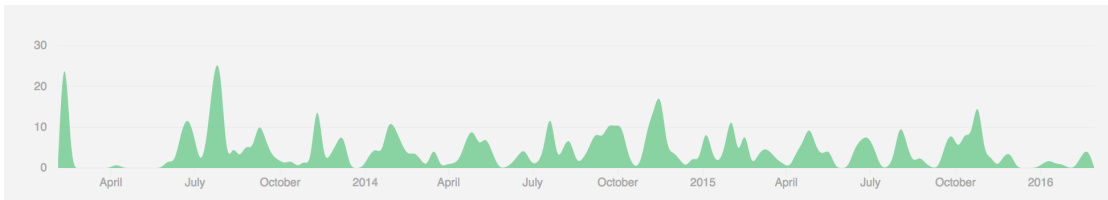


FIGURE 3.4: Commit history from Feb 3, 2013 to Feb 29, 2016, showing the regular code development that makes version control such a necessity to a collaborative code project. Produced using the Github API and plotting capability.

The densities in the model are then multiplied by this factor. This has the effect of enhancing ‘ ρ^2 ’ processes such as recombination or collisional excitation, and

3.9 Code Validation

The main challenge for high performance scientific computing can be elegantly summarised by Ferland’s (2002) epitaph, ‘*Reliability in the face of complexity*’. I have already delved into some of the complexity in this case, so it is important to assess whether the code is also reliable before I present results.

3.9.1 Testing against Cloudy

3.9.2 Testing against Tardis

3.10 Code Maintenance and Version Control

As part of the expansion of the team working on PYTHON I was responsible for bringing the code under the auspices of a robust version control system. Thanks to these efforts, the code is now hosted on GitHub at <https://github.com/agnwinds/python/>. Our team uses a Pull & Fork model for collaborative code development, in which major changes are made in a forked repository before the developer submits a ‘Pull request’ to the main repository. To test the code, we use a combination of Travis CI build tests – run per commit to the upstream repo – and our own test suite which is run every night on a multi-core server.

3.10.1 Parallelisation

Bibliography

- Allen, J. T., P. C. Hewett, N. Maddox, G. T. Richards, and V. Belokurov
2011. A strong redshift dependence of the broad absorption line quasar fraction.
MNRAS, 410:860–884.
- Angel, J. R. P. and H. S. Stockman
1980. Optical and infrared polarization of active extragalactic objects. *ARA&A*, 18:321–361.
- Antonucci, R. R. J. and J. S. Miller
1985. Spectropolarimetry and the nature of NGC 1068. *ApJ*, 297:621–632.
- Arévalo, P. and P. Uttley
2006. Investigating a fluctuating-accretion model for the spectral-timing properties of accreting black hole systems. *MNRAS*, 367:801–814.
- Bartlett, E.
2013. *High mass X-ray binaries in the Milky Way and beyond: a multiwavelength temporal and spectroscopic study*. PhD thesis, University of Southampton.
- Begelman, M. C., A. C. Fabian, and M. J. Rees
2008. Implications of very rapid TeV variability in blazars. *MNRAS*, 384:L19–L23.
- Begelman, M. C., C. F. McKee, and G. A. Shields
1983. Compton heated winds and coronae above accretion disks. I Dynamics. *ApJ*, 271:70–88.
- Belloni, T., ed.
2010. *The Jet Paradigm*, volume 794 of *Lecture Notes in Physics*, Berlin Springer Verlag.
- Benz, A. O., E. Fuerst, and A. L. Kiplinger
1983. First detection of radio emission from a dwarf nova. *Nature*, 302:45.
- Bondi, H.
1952. On spherically symmetrical accretion. *MNRAS*, 112:195.

- Bondi, H. and F. Hoyle
1944. On the mechanism of accretion by stars. *MNRAS*, 104:273.
- Cassinelli, J. P.
1979. Stellar winds. *ARAA*, 17:275–308.
- Cohen, R. D., R. C. Puetter, R. J. Rudy, T. B. Ake, and C. B. Foltz
1986. Variability of Markarian 1018 - Seyfert 1.9 to Seyfert 1. *ApJ*, 311:135–141.
- Coppejans, D. L., E. G. Körding, J. C. A. Miller-Jones, M. P. Rupen, C. Knigge, G. R. Sivakoff, and P. J. Groot
2015. Novalike cataclysmic variables are significant radio emitters. *MNRAS*, 451:3801–3813.
- Cordova, F. A. and K. O. Mason
1982. High-velocity winds from a dwarf nova during outburst. *ApJ*, 260:716–721.
- Denney, K. D., G. De Rosa, K. Croxall, A. Gupta, M. C. Bentz, M. M. Fausnaugh, C. J. Grier, P. Martini, S. Mathur, B. M. Peterson, R. W. Pogge, and B. J. Shappee
2014. The Typecasting of Active Galactic Nuclei: Mrk 590 no Longer Fits the Role. *ApJ*, 796:134.
- Dexter, J. and E. Agol
2011. Quasar Accretion Disks are Strongly Inhomogeneous. *ApJ Letters*, 727:L24.
- Dhillon, V. S.
1996. The Nova-like variables. In *IAU Colloq. 158: Cataclysmic Variables and Related Objects*, A. Evans and J. H. Wood, eds., volume 208 of *Astrophysics and Space Science Library*, P. 3.
- Díaz Trigo, M. and L. Boirin
2015. Accretion disc atmospheres and winds in low-mass X-ray binaries. *ArXiv e-prints*.
- Edelson, R., J. M. Gelbord, K. Horne, I. M. McHardy, B. M. Peterson, P. Arévalo, A. A. Breeveld, G. De Rosa, P. A. Evans, M. R. Goad, G. A. Kriss, W. N. Brandt, N. Gehrels, D. Grupe, J. A. Kennea, C. S. Kochanek, J. A. Nousek, I. Papadakis, M. Siegel, D. Starkey, P. Uttley, S. Vaughan, S. Young, A. J. Barth, M. C. Bentz, B. J. Brewer, D. M. Crenshaw, E. Dalla Bontà, A. De Lorenzo-Cáceres, K. D. Denney, M. Dietrich, J. Ely, M. M. Fausnaugh, C. J. Grier, P. B. Hall, J. Kaastra, B. C. Kelly, K. T. Korista, P. Lira, S. Mathur, H. Netzer, A. Pancoast, L. Pei, R. W. Pogge, J. S. Schimoia, T. Treu, M. Vestergaard, C. Villforth, H. Yan, and Y. Zu
2015. Space Telescope and Optical Reverberation Mapping Project. II. Swift and HST Reverberation Mapping of the Accretion Disk of NGC 5548. *ApJ*, 806:129.

- Edge, D. O., J. R. Shakeshaft, W. B. McAdam, J. E. Baldwin, and S. Archer
1959. A survey of radio sources at a frequency of 159 Mc/s. *MmRA*, 68:37–60.
- Eggleton, P. P.
1983. Approximations to the radii of Roche lobes. *ApJ*, 268:368.
- Ehman, J. R., R. S. Dixon, and J. D. Kraus
1970. The Ohio survey between declinations of 0 and 36 south. *AJ*, 75:351–506.
- Ekers, J. A.
1969. The Parkes catalogue of radio sources, declination zone +20 to -90 . *Australian Journal of Physics Astrophysical Supplement*, 7.
- Elitzur, M.
2012. On the Unification of Active Galactic Nuclei. *ApJ Letters*, 747:L33.
- Elitzur, M., L. C. Ho, and J. R. Trump
2014. Evolution of broad-line emission from active galactic nuclei. *MNRAS*, 438:3340–3351.
- Elvis, M.
2000. A Structure for Quasars. *ApJ*, 545:63–76.
- Elvis, M., B. J. Wilkes, J. C. McDowell, R. F. Green, J. Bechtold, S. P. Willner, M. S. Oey, E. Polomski, and R. Cutri
1994. Atlas of quasar energy distributions. *ApJs*, 95:1–68.
- Fabian, A. C.
2012. Observational Evidence of Active Galactic Nuclei Feedback. *ARA&A*, 50:455–489.
- Falomo, R., E. Pian, and A. Treves
2014. An optical view of BL Lacertae objects. *AAPR*, 22:73.
- Fanaroff, B. L. and J. M. Riley
1974. The morphology of extragalactic radio sources of high and low luminosity. *MNRAS*, 167:31P–36P.
- Fath, E. A.
1909. The spectra of some spiral nebulae and globular star clusters. *Lick Observatory Bulletin*, 5:71–77.
- Fender, R. P.
2001. Powerful jets from black hole X-ray binaries in low/hard X-ray states. *MNRAS*, 322:31–42.

- Frank, J., A. King, and D. Raine
1992. *Accretion power in astrophysics.*
- Ghisellini, G., L. Maraschi, and A. Treves
1985. Inhomogeneous synchrotron-self-Compton models and the problem of relativistic beaming of BL Lac objects. *A&A*, 146:204–212.
- Ghisellini, G., P. Padovani, A. Celotti, and L. Maraschi
1993. Relativistic bulk motion in active galactic nuclei. *ApJ*, 407:65–82.
- Greenstein, J. L. and J. B. Oke
1982. RW Sextantis, a disk with a hot, high-velocity wind. *ApJ*, 258:209–216.
- Gültekin, K., D. O. Richstone, K. Gebhardt, T. R. Lauer, S. Tremaine, M. C. Aller, R. Bender, A. Dressler, S. M. Faber, A. V. Filippenko, R. Green, L. C. Ho, J. Kormendy, J. Magorrian, J. Pinkney, and C. Siopis
2009. The M- σ and M-L Relations in Galactic Bulges, and Determinations of Their Intrinsic Scatter. *ApJ*, 698:198–221.
- Hamann, W.-R. and L. Koesterke
1998. Spectrum formation in clumped stellar winds: consequences for the analyses of Wolf-Rayet spectra. *A&A*, 335:1003–1008.
- Hamann, W.-R., L. M. Oschinova, and A. Feldmeier
2008. Spectrum formation in clumpy stellar winds. In *Clumping in Hot-Star Winds*, W.-R. Hamann, A. Feldmeier, and L. M. Oschinova, eds., P. 75.
- Häring, N. and H.-W. Rix
2004. On the Black Hole Mass-Bulge Mass Relation. *ApJ Letters*, 604:L89–L92.
- Hassall, B. J. M.
1985. A superoutburst of the dwarf nova EK Trianguli Australis. *MNRAS*, 216:335–352.
- Haug, K.
1987. Continuum distributions and line profiles of UX UMa-type novalike systems. *AP&SS*, 130:91–102.
- Hazard, C., M. B. Mackey, and A. J. Shimmins
1963. Investigation of the Radio Source 3C 273 By The Method of Lunar Occultations. *Nature*, 197:1037–1039.
- Heap, S. R., A. Boggess, A. Holm, D. A. Klinglesmith, W. Sparks, D. West, C. C. Wu, A. Boksenberg, A. Willis, R. Wilson, F. Macchetto, P. O. Selvelli, D. Stickland, J. L.

- Greenstein, J. B. Hutchings, A. B. Underhill, R. Viotti, and J. A. J. Whelan
1978. IUE observations of hot stars - HZ43, BD +75 deg 325, NGC 6826, SS Cygni,
Eta Carinae. *Nature*, 275:385–388.
- Heil, L. M., S. Vaughan, and P. Uttley
2012. The ubiquity of the rms-flux relation in black hole X-ray binaries. *MNRAS*,
422:2620–2631.
- Hessman, F. V., E. L. Robinson, R. E. Nather, and E.-H. Zhang
1984. Time-resolved spectroscopy of SS Cygni at minimum and maximum light. *ApJ*,
286:747–759.
- Higginbottom, N., C. Knigge, K. S. Long, S. A. Sim, and J. H. Matthews
2013. A simple disc wind model for broad absorption line quasars. *MNRAS*, 436:1390–
1407.
- Hillier, D. J. and D. L. Miller
1999. Constraints on the Evolution of Massive Stars through Spectral Analysis. I. The
WC5 Star HD 165763. *ApJ*, 519:354–371.
- Hoffmeister, C.
1929. 354 neue Veränderliche. *Astronomische Nachrichten*, 236:233.
- Hogg, J. D. and C. Reynolds
2015. Testing the Propagating Fluctuations Model with a Long, Global Accretion
Disk Simulation. *ArXiv e-prints*.
- Hönig, S. F., M. Kishimoto, K. R. W. Tristram, M. A. Prieto, P. Gandhi, D. Asmus,
R. Antonucci, L. Burtscher, W. J. Duschl, and G. Weigelt
2013. Dust in the Polar Region as a Major Contributor to the Infrared Emission of
Active Galactic Nuclei. *ApJ*, 771:87.
- Horne, K.
1993. *Eclipse Mapping of Accretion Disks: The First Decade*, P. 117.
- Hoyle, F. and R. A. Lyttleton
1939. The effect of interstellar matter on climatic variation. *Proceedings of the Cam-
bridge Philosophical Society*, 35:405.
- Idan, I., J.-P. Lasota, J.-M. Hameury, and G. Shaviv
2010. Accretion-disc model spectra for dwarf-nova stars. *A&A*, 519:A117.
- Kafka, S. and R. K. Honeycutt
2004. Detecting Outflows from Cataclysmic Variables in the Optical. *AJ*, 128:2420–
2429.

- Kerzendorf, W. E. and S. A. Sim
2014. A spectral synthesis code for rapid modelling of supernovae. *MNRAS*, 440:387–404.
- King, A.
2003. Black Holes, Galaxy Formation, and the M_{BH} - σ Relation. *ApJ Letters*, 596:L27–L29.
- Knigge, C., K. S. Long, R. A. Wade, R. Baptista, K. Horne, I. Hubeny, and R. G. M. Rutten
1998a. Hubble Space Telescope Eclipse Observations of the Nova-like Cataclysmic Variable UX Ursae Majoris. *ApJ*, 499:414–428.
- Knigge, C., K. S. Long, R. A. Wade, R. Baptista, K. Horne, I. Hubeny, and R. G. M. Rutten
1998b. Hubble Space Telescope Eclipse Observations of the Nova-like Cataclysmic Variable UX Ursae Majoris. *ApJ*, 499:414.
- Knigge, C., S. Scaringi, M. R. Goad, and C. E. Cottis
2008. The intrinsic fraction of broad-absorption line quasars. *MNRAS*, 386:1426–1435.
- Körding, E., M. Rupen, C. Knigge, R. Fender, V. Dhawan, M. Templeton, and T. Muxlow
2008. A Transient Radio Jet in an Erupting Dwarf Nova. *Science*, 320:1318–.
- Kotov, O., E. Churazov, and M. Gilfanov
2001. On the X-ray time-lags in the black hole candidates. *MNRAS*, 327:799–807.
- Krolik, J. H. and M. C. Begelman
1986. The Dynamical State of the Obscuring Torus in Seyfert Galaxies. In *Bulletin of the American Astronomical Society*, volume 18 of *BAAS*, P. 903.
- Kromer, M. and S. A. Sim
2009. Time-dependent three-dimensional spectrum synthesis for Type Ia supernovae. *MNRAS*, 398:1809–1826.
- Kuulkers, E., S. Motta, J. Kajava, J. Homan, R. Fender, and P. Jonker
2015. Renewed activity of V404 Cyg (GS 2023+338). *The Astronomer's Telegram*, 7647.
- La Dous, C.
1989. On the Balmer jump in dwarf novae during the outburst. *MNRAS*, 238:935–943.

- Lasota, J.-P.
2001. The disc instability model of dwarf novae and low-mass X-ray binary transients. *NAR*, 45:449–508.
- Liebert, J. and H. S. Stockman
1985. The AM Herculis magnetic variables. In *Cataclysmic Variables and Low-Mass X-ray Binaries*, D. Q. Lamb and J. Patterson, eds., volume 113 of *Astrophysics and Space Science Library*, Pp. 151–177.
- Long, K. S., W. P. Blair, A. F. Davidsen, C. W. Bowers, W. V. D. Dixon, S. T. Durrance, P. D. Feldman, R. C. Henry, G. A. Kriss, J. W. Kruk, H. W. Moos, O. Vancura, H. C. Ferguson, and R. A. Kimble
1991. Spectroscopy of Z Camelopardalis in outburst with the Hopkins Ultraviolet Telescope. *ApJ Letters*, 381:L25–L29.
- Long, K. S., R. A. Wade, W. P. Blair, A. F. Davidsen, and I. Hubeny
1994. Observations of the bright novalike variable IX Velorum with the Hopkins Ultraviolet Telescope. *ApJ*, 426:704–715.
- Lucy, L. B.
2002. Monte Carlo transition probabilities. *A&A*, 384:725–735.
- Lucy, L. B.
2003. Monte Carlo transition probabilities. II. *A&A*, 403:261–275.
- Lynden-Bell, D.
1969. Galactic Nuclei as Collapsed Old Quasars. *Nature*, 223:690–694.
- Lyubarskii, Y. E.
1997. Flicker noise in accretion discs. *MNRAS*, 292:679.
- Marinucci, A., S. Bianchi, G. Matt, D. M. Alexander, M. Baloković, F. E. Bauer, W. N. Brandt, P. Gandhi, M. Guainazzi, F. A. Harrison, K. Iwasawa, M. Koss, K. K. Madsen, F. Nicastro, S. Puccetti, C. Ricci, D. Stern, and D. J. Walton
2016. NuSTAR catches the unveiling nucleus of NGC 1068. *MNRAS*, 456:L94–L98.
- Marscher, A. P.
2006. Relativistic Jets in Active Galactic Nuclei. In *Relativistic Jets: The Common Physics of AGN, Microquasars, and Gamma-Ray Bursts*, P. A. Hughes and J. N. Bregman, eds., volume 856 of *American Institute of Physics Conference Series*, Pp. 1–22.
- Matt, G., M. Guainazzi, and R. Maiolino
2003. Changing look: from Compton-thick to Compton-thin, or the rebirth of fossil active galactic nuclei. *MNRAS*, 342:422–426.

- McConnell, N. J. and C.-P. Ma
2013. Revisiting the Scaling Relations of Black Hole Masses and Host Galaxy Properties. *ApJ*, 764:184.
- McHardy, I. M., E. Koerding, C. Knigge, P. Uttley, and R. P. Fender
2006. Active galactic nuclei as scaled-up Galactic black holes. *Nature*, 444:730–732.
- Morgan, C. W., C. S. Kochanek, N. D. Morgan, and E. E. Falco
2010. The Quasar Accretion Disk Size-Black Hole Mass Relation. *ApJ*, 712:1129–1136.
- Motta, S., A. Beardmore, S. Oates, N. P. M. K. A. Sanna, E. Kuulkers, J. Kajava, and C. Sanchez-Fernandez
2015. X-ray and optical/UV variability from V404 Cyg (GS 2023+338) observed by Swift (part 1 of 2). *The Astronomer’s Telegram*, 7665.
- Murray, N., J. Chiang, S. A. Grossman, and G. M. Voit
1995. Accretion Disk Winds from Active Galactic Nuclei. *ApJ*, 451:498.
- Neugebauer, G., J. B. Oke, E. E. Becklin, and K. Matthews
1979. Absolute spectral energy distribution of quasi-stellar objects from 0.3 to 10 microns. *ApJ*, 230:79–94.
- Orr, M. J. L. and I. W. A. Browne
1982. Relativistic beaming and quasar statistics. *MNRAS*, 200:1067–1080.
- Patterson, J.
1994. The DQ Herculis stars. *PASP*, 106:209–238.
- Patterson, J., R. Patino, J. R. Thorstensen, D. Harvey, D. R. Skillman, and F. A. Ringwald
1996. Periods and Quasiperiods in the Cataclysmic Variable BZ Camelopardalis. *AJ*, 111:2422.
- Perley, R. A., J. W. Dreher, and J. J. Cowan
1984. The jet and filaments in Cygnus A. *ApJ Letters*, 285:L35–L38.
- Ponti, G., R. P. Fender, M. C. Begelman, R. J. H. Dunn, J. Neilsen, and M. Coriat
2012. Ubiquitous equatorial accretion disc winds in black hole soft states. *MNRAS*, 422:L11.
- Potash, R. I. and J. F. C. Wardle
1980. 4C 32.69 - A quasar with a radio jet. *ApJ*, 239:42–49.
- Pounds, K. A. and J. N. Reeves
2009. Quantifying the fast outflow in the luminous Seyfert galaxy PG1211+143. *MNRAS*, 397:249–257.

- Puccetti, S., F. Fiore, G. Risaliti, M. Capalbi, M. Elvis, and F. Nicastro
2007. Rapid N_H changes in NGC 4151. *MNRAS*, 377:607–616.
- Reeves, J. N., P. T. O'Brien, and M. J. Ward
2003. A Massive X-Ray Outflow from the Quasar PDS 456. *ApJ Letters*, 593:L65–L68.
- Ringwald, F. A. and T. Naylor
1998. High-speed optical spectroscopy of a cataclysmic variable wind - BZ Camelopardalis. *AJ*, 115:286.
- Rottenberg, J. A.
1952. Theoretical line profiles for stars of P Cygni type. *MNRAS*, 112:125.
- Rutten, R. G. M., J. van Paradijs, and J. Tinbergen
1992. Reconstruction of the accretion disk in six cataclysmic variable stars. *A&A*, 260:213–226.
- Scaringi, S., E. Körding, P. Uttley, C. Knigge, P. J. Groot, and M. Still
2012. The universal nature of accretion-induced variability: the rms-flux relation in an accreting white dwarf. *MNRAS*, 421:2854–2860.
- Scaringi, S., T. J. Maccarone, E. Koerding, C. Knigge, S. Vaughan, T. R. Marsh,
E. Aranzana, V. Dhillon, and S. C. C. Barros
2015. Accretion-induced variability links young stellar objects, white dwarfs, and black holes. *ArXiv e-prints*.
- Seyfert, C. K.
1943. Nuclear Emission in Spiral Nebulae. *ApJ*, 97:28.
- Shakura, N. I. and R. A. Sunyaev
1973. Black holes in binary systems. Observational appearance. *A&A*, 24:337–355.
- Shaviv, G. and R. Wehrse
1991. Continuous energy distributions of accretion discs. *A&A*, 251:117–132.
- Silk, J. and M. J. Rees
1998. Quasars and galaxy formation. *A&A*, 331:L1–L4.
- Sim, S. A.
2004. Mass-loss rates for hot luminous stars: the influence of line branching. *MNRAS*, 349:899–908.
- Sim, S. A., J. E. Drew, and K. S. Long
2005. Two-dimensional Monte Carlo simulations of HI line formation in massive young stellar object disc winds. *MNRAS*, 363:615–627.

- Sim, S. A., K. S. Long, L. Miller, and T. J. Turner
2008. Multidimensional modelling of X-ray spectra for AGN accretion disc outflows. *MNRAS*, 388:611–624.
- Springel, V., T. Di Matteo, and L. Hernquist
2005. Black Holes in Galaxy Mergers: The Formation of Red Elliptical Galaxies. *ApJ Letters*, 620:L79–L82.
- Struve, O.
1935. The Spectrum of P Cygni. *ApJ*, 81:66.
- Tatum, M. M., T. J. Turner, S. A. Sim, L. Miller, J. N. Reeves, A. R. Patrick, and K. S. Long
2012. Modeling the Fe K Line Profiles in Type I Active Galactic Nuclei with a Compton-thick Disk Wind. *ApJ*, 752:94.
- Tohline, J. E. and D. E. Osterbrock
1976. Variation of the spectrum of the Seyfert galaxy NGC 7603. *ApJ Letters*, 210:L117–L120.
- Tombesi, F., M. Cappi, J. N. Reeves, G. G. C. Palumbo, T. Yaqoob, V. Braito, and M. Dadina
2010. Evidence for ultra-fast outflows in radio-quiet AGNs. I. Detection and statistical incidence of Fe K-shell absorption lines. *A&A*, 521:A57.
- Urry, C. M. and P. Padovani
1995. Unified Schemes for Radio-Loud Active Galactic Nuclei. *PASP*, 107:803.
- Uttley, P. and I. M. McHardy
2001. The flux-dependent amplitude of broadband noise variability in X-ray binaries and active galaxies. *MNRAS*, 323:L26–L30.
- Uttley, P., I. M. McHardy, and S. Vaughan
2005. Non-linear X-ray variability in X-ray binaries and active galaxies. *MNRAS*, 359:345–362.
- Van de Sande, M., S. Scaringi, and C. Knigge
2015. The rms-flux relation in accreting white dwarfs: another nova-like variable and the first dwarf nova. *MNRAS*, 448:2430–2437.
- Wade, R. A.
1984. A double grid of accretion disc model spectra for cataclysmic variable stars. *MNRAS*, 208:381–398.

- Wade, R. A.
1988. A test of synthetic accretion disk spectra using ultraviolet flux distributions of novalike variables. *ApJ*, 335:394–405.
- Warner, B.
2003. *Cataclysmic Variable Stars*.
- Weymann, R. J., S. L. Morris, C. B. Foltz, and P. C. Hewett
1991. Comparisons of the emission-line and continuum properties of broad absorption line and normal quasi-stellar objects. *ApJ*, 373:23–53.
- Wills, B. J. and M. S. Brotherton
1995. An Improved Measure of Quasar Orientation. *ApJ Letters*, 448:L81.
- Woltjer, L.
1959. Emission Nuclei in Galaxies. *ApJ*, 130:38.
- Woods, D. T., R. I. Klein, J. I. Castor, C. F. McKee, and J. B. Bell
1996. X-Ray-heated Coronae and Winds from Accretion Disks: Time-dependent Two-dimensional Hydrodynamics with Adaptive Mesh Refinement. *ApJ*, 461:767.
- Woods, J. A.
1991. PhD thesis, D. Phil thesis, Univ. Oxford , (1991).
- Wright, S. C., I. M. McHardy, and R. G. Abraham
1998. Host galaxies of the optically violently variable quasars PKS 0736+017, OJ 287 and LB 2136. *MNRAS*, 295:799–812.